Institute for Advanced Technology
The University of Texas at Austin

Analysis of the Armature-Rail Interface in Solid Armature Railguns

Collected Reports of Professor L. C. Woods
(October 1995 — June 1996)

L. C. Woods
Institute for Advanced Technology
The University of Texas at Austin

August 1996

IAT.R 0120

Certificate of Technical Review

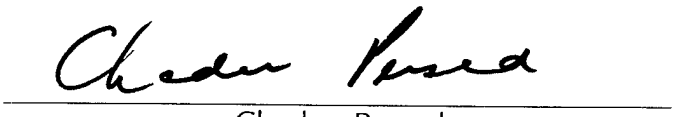

Chadee Persad

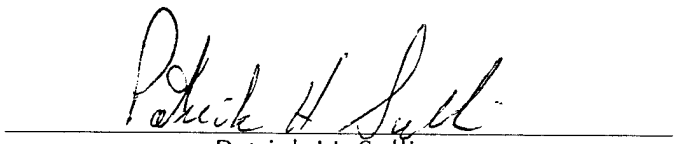

Patrick H. Sullivan

REPORT DOCUMENTATION PAGE

Form Approved
OMB NO. 0704-0188

1. AGENCY USE ONLY (Leave blank)	2. REPORT DATE	3. REPORT TYPE AND DATES COVERED
	August 1996	Technical Report, Oct 1995 - June 1996

4. TITLE AND SUBTITLE

Analysis of the Armature-Rail Interface in Solid Armature Railguns: Collected Reports of Professor L. C. Woods (October 1995 — June 1996)

5. FUNDING NUMBERS

Contract # DAAA21-93-C-0101

6. AUTHOR(S)

L. C. Woods

7. PERFORMING ORGANIZATION NAME(S) AND ADDRESS(ES)

Institute for Advanced Technology
The University of Texas at Austin
4030-2 W. Braker Lane, #200
Austin, TX 78759

8. PERFORMING ORGANIZATION REPORT NUMBER

IAT.R 0120

9. SPONSORING / MONITORING AGENCY NAME(S) AND ADDRESS(ES)

U.S. Army Research Laboratory
ATTN: AMSRL-WT-T
Aberdeen Proving Ground, MD 21005-5066

10. SPONSORING / MONITORING AGENCY REPORT NUMBER

11. SUPPLEMENTARY NOTES

The view, opinions and/or findings contained in this report are those of the author(s) and should not be considered as an official Department of the Army position, policy, or decision, unless so designated by other documentation.

12a. DISTRIBUTION / AVAILABILITY STATEMENT

Approved for public release; distribution unlimited.

12b. DISTRIBUTION CODE

A

13. ABSTRACT *(Maximum 200 words)*

A collection of reports written by L.C. Woods for the Institute for Advanced Technology (IAT), University of Texas at Austin, investigating the liquid metal interface between a solid armature and conducting rail of an electromagnetic launcher as it effects transition and gouging. In the first report, a two-dimensional current melt-wave model is presented that provides a datum against which observations and numerical modeling can be compared. The second report removes some of the initial assumptions and replaces the ideal model of electrical contact by the contact-spot model. The third report replaces the dimensional arguments used in the first report to obtain the scale lengths for the current distributions with a mathematical solution. The fourth report utilizes beam theory to investigate the critical velocity at which rail gouging is likely to begin. Report five provides a description of how one might set up an efficient numerical treatment that allows for both three-dimensional effects and time dependence. The final report concludes with an explanation of the transverse striations that have been observed with aluminum rails.

14. SUBJECT TERMS

Armature, transition, gouging, current melt wave theory, current melt wave model, contact-spot model, armature / rail interface, railgun, electromagnetic launcher.

15. NUMBER OF PAGES

66

16. PRICE CODE

17. SECURITY CLASSIFICATION OF REPORT	18. SECURITY CLASSIFICATION OF THIS PAGE	19. SECURITY CLASSIFICATION OF ABSTRACT	20. LIMITATION OF ABSTRACT
Unclassified	Unclassified	Unclassified	UL

NSN 7540-01-280-5500

Standard Form 298 (Rev.2-89)
Prescribed by ANSI Std. 239-18 298-102

TABLE OF CONTENTS

Preface

The reports written by L.C. Woods for the Institute for Advanced Technology (IAT), University of Texas at Austin, and collected together here are:

1. "The Current Melt-Wave Model," October, 1995
2. "The Contact-Spot Model of Transition," December, 1995
3. "Paper for the 8th EML Symposium," January, 1996
4. "An Armature/Rail Instability," February, 1996
5. "Three-Dimensional Effects on the Melt-Wave Model," May, 1996
6. "Boundary Conditions Across a Rail/Armature Contact Surface," June, 1996

A brief survey of their contents and relationships follow.

1. The research started with a rather idealised model of the interaction between a rail and a solid armature. It is a two-dimensional model and the electrical contact between the surfaces is assumed to be ideal. The main result is an expression for the velocity v_m at which a melt wave advances along the armature interface. It was based on the assumption that the depth h, of the molten layer, assumed to be removed by the viscous force due to the rail, is equal to the scale-length of the current density. Alternatively, one might have taken h to be equal to the thermal skin depth. Short of a complete numerical calculation, it was difficult to decide between these two possibilities. Transition was assumed to occur when the melt wave reached the end of the armature surface in contact with the rail. The merit of an ideal model, besides its simplicity, is that it gives a datum against which observations and numerical modeling can be compared.

2. The second report removes some of the assumptions adopted in (1), and also replaces the ideal model of electrical contact by the contact-spot model. The latter assumes that the electricity flows across the interface between the rail and armature through small, isolated spots, known as "a-spots." The adiabatic assumption made by earlier workers was replaced by a diathermic model in which heat transport played an important role. Transition was deemed to have occurred when all the spots were "burnt out." One important variable that was difficult to determine is ε, the ratio of the conducting area of the spots to the actual area of the armature face.

3. This report was largely a revised version of (1), prepared for the 8th EML Symposium in Baltimore, held last April. The main change was that the dimensional arguments used in (1) to obtain the scale lengths for the current distributions, were replaced by a mathematical solution. This was obtained by using rectangular geometry for the armature, which is not a good representation of the actual shapes employed. However, as the main purpose was simply to provide a more convincing derivation of the scale-lengths (valid in any geometry), this was not a real restriction. Transition was defined to occur when the melt wave had removed sufficient material to eliminate the normal force between the rail and the armature. This was more reasonable than the definition adopted in (1) and also had the advantage that the uncertain depth h no longer played a role, since transition now depended on the product h which is independent of the mechanism assumed to be responsible for hv_m alone.

4. The movement of a load along a beam, supported on an elastic foundation, can excite the beam into transverse vibrations that have a large amplitude when the speed of the load is close to the velocity of free waves along the beam. In this report, This idea was applied to the rail/armature combination, with a view to finding an explanation of the critical velocity at which rail gouging was likely to begin. The main problem was to determine the response of the elastic foundation to a distributed load. For aluminum armatures a critical velocity of about 1,400 m/s was found, which is close to that observed. This occurred with symmetrical displacements of the rails. With the much heavier copper armatures, to obtain results close to experimental values, it was necessary to assume the displacements to be axisymmetrical. This gave value of the critical velocity of about 600 m/s, also close to experiment. This work was aimed at explaining the onset of gouging, not the details of the actual process.

5. Because the electric current has a tendency to flow over the edges of the armature, the two-dimensional assumption fails at these edges. The result is that the melt wave travels much faster near these boundaries. The report contains an attempt to obtain a simple physical model of the phenomenon, avoiding the expense of an extensive computer calculation. The main result is an expression for the speed of the melt wave as a function of the distance measured across the armature. The report concluded with a description of how one might set up an efficient numerical treatment that allows for both three-dimensional effects and time dependence.

6. In this report it is argued that the current is carried though the interface, mainly by the penetration of the copper asperities into the softer aluminum. The relative motion of the surfaces allows the asperities to "plough" the aluminum, which action generates conducting streaks, that merge into a continuous melt wave. The main change to the melt wave model of (1) is that the expression for the electrical resistivity is somewhat larger, since it takes into account some features of the spot model. The report concluded with an explanation of the transverse striations that have been observed with aluminum rails. They are attributed to the instability of the vortex sheet formed by the melted material between the sliding surfaces.

This work was supported by the U.S. Army Research Laboratory (ARL) under contract DAAA21-93-C-0101.

Professor L.C. Woods
August, 1996

Progress Report on Research into Electromagnetic Launchers

The Current Melt-Wave Model

October 1995

Professor L. C. Woods
University of Oxford
Mathematical Institute

The Current Melt-Wave Model

Summary

It is generally accepted that the velocity skin effect concentrates the current crossing the armature/rail interface at the rear corners of a solid armature. Ohmic heating melts these corners and since the resisitivity of the liquid phase exceeds that of the solid phase, the current is deflected forwards into the solid region. The mechanism results in a 'melt-wave' moving from the back to the front of the armature. There are two distinct descriptions for this process, the entrainment model and the liquid model. In the first of these, shown in Fig. 1, the molten metal is quickly removed by entrainment on the rails. This leaves a high resistance vapour or plasma gap between the armature and the rails. In the liquid model, shown in Fig. 2, the armature/rail interface is initially filled with molten metal, with vaporisation occurring at a later stage. Since the completion of vaporisation along the interface greatly increases the resistivity, the efficiency of the rail-gun depends on delaying this process as much as possible. It is therefore important to choose a model of the melt-wave that accurately represents the physical situation. The speed v_m at which the melt wave advances relative to the armature, is a key parameter. If v_m is relatively large, then the transition from metal-to-metal contact to a plasma contact layer occurs early and the velocity V attainable by the armature is restricted.

An expression for v_m can be deduced from the energy equation applied to the solid region of the armature extending in front of the melt wave. We shall show that it is related to V by

$$v_m = \frac{\overline{\eta}_a}{4\eta_r}\frac{\mu_0 I^2 V}{\rho Q w^2} - v_\kappa\,, \tag{1}$$

where

$$v_\kappa \equiv \frac{\mu_0 \kappa_a}{\rho Q \overline{\eta}_a}(T_m - T_0)V, \qquad Q \equiv c_p(T_m - T_0) + L_m\,. \tag{2}$$

In these expressions $\overline{\eta}_a$ is an average resistivity in the solid armature, η_r is the rail resistivity, μ_0 is the permeability of free space, I is the total current flowing through the armature, ρ is the armature density, w is the depth of the surface of the armature in contact with a rail, T_m is the melting temperature, T_0 is the laboratory temperature, L_m is the enthalpy of fusion (latent heat), c_p is the specific heat at constant pressure and κ_a is the thermal conductivity in the armature. In §5 we shall use (1) to derive a limiting speed V_c for the armature.

To decide between the models, we first need to determine whether or not the rate of increase of the volume of the metal at melting is greater or smaller than the rate at which it is removed by entrainment. For the liquid model to be acceptable, the first of these rates must exceed the second. If this criterion is met, we then need to determine whether or not the net force acting on the liquid phase is directed towards the armature or not. If not, then the solid armature can accelerate away from its liquid phase.

Finally we present a critical review of work by Parks[1] on the entrainment model, and by James[2] on the liquid model. Their expressions for v_m disagree with each others and also with ours. We shall also consider a work by Barber and Challita[3], who introduce a quite different approach to the problem of transition, one that challenges the validity of either the entrainment or liquid models.

1. Introduction

Referring to Figs. 1 and 2, we note that in the entrainment model there is no current flowing across the gap below CD, whereas in the liquid model, provided the conductivity of the liquid phase is not much larger than that of the solid phase, there will be some current flowing. Let R denote the ratio of the resistivity of the liquid phase to the solid phase, then R will play a role in determining the shape of the region of the liquid phase, shown in more detail in Fig. 3. With Aluminium alloy, R = 2.4, whereas with Titanium, R = 26. Therefore in the latter case there will be very little current flowing across the liquid and the melted region will have a shape more like that shown in Fig. 1 for the entrainment model.

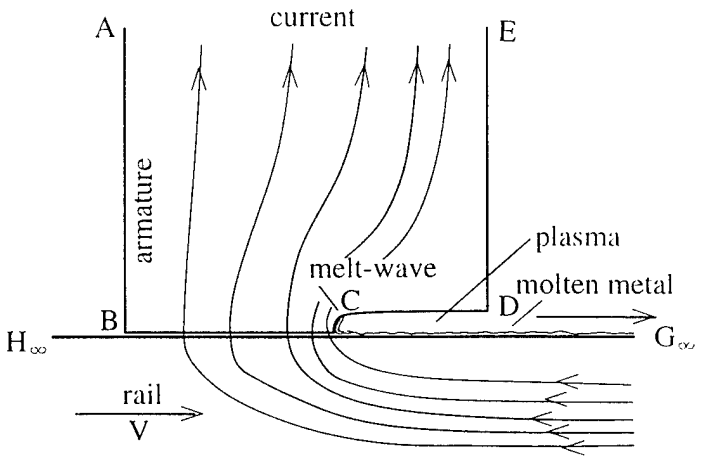

Figure 1: Entrainment model

First consider the case illustrated in Fig. 2 and in more detail in Fig. 3. As the surface CD moves forward, increasing the volume of the liquid phase, either the liquid remains with the armature, lubricating its motion along the rail, or it is removed so fast by the friction force acting on it, that a plasma gap is formed and the liquid model is replaced by

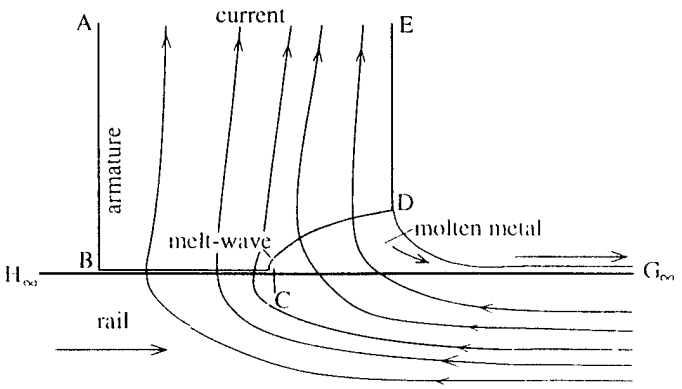

Figure 2: Liquid model

the entrainment model. We shall adopt a coordinate system F fixed in the solid armature. The rail, lying below the surface $H_\infty G_\infty$, moves with a velocity V to the right. It also has an acceleration $\dot{V}$ in the same direction. Viewed from F, there are no net forces acting on the solid armature, but the liquid phase will be subject to a surface friction force along CG_∞ and a volume distributed electromagnetic force, with a component in the opposite direction. Granted that the melt-wave creates enough liquid to offset the frictional losses, to decide between the two models, we need estimates of the magnitude of these forces.

A related problem is the distribution of the electric current in the solid and liquid phases of the armature, for this will determine both the rate at which the armature is transformed into the liquid phase by ohmic heating and the magnitude of the EM force tending to maintain the molten metal in position, adhering to the solid armature.

The location of the field depends on the time available for it to diffuse towards its equilibrium state. The time τ_ℓ for the field to diffuse through a distance ℓ is

$$\tau_\ell = \ell^2/\xi\,, \qquad \xi \equiv \eta/\mu_0\,. \qquad (\mu_0 = 4\pi \times 10^{-7}), \tag{3}$$

where η is the resistivity and ξ is the magnetic (or resistive) diffusivity. And as the diffusion time is smaller in the melted material than in the solid, once the melting begins, the field will diffuse more rapidly through it. As this happens, the EM force acting on the liquid phase — designated by $\mathcal{L}$ in the following — is rapidly reduced. But even if the liquid phase had the same resistivity as the solid phase, the penetration of the magnetic field into the armature would mean that the *total* force acting on $\mathcal{L}$ would be reduced, since the elastic stresses are absent in $\mathcal{L}$. For liquid Aluminium alloy $\tau_\ell \approx 16\ell^2$, i.e. for an armature depth of 10 mm this time is 1.6 ms and the half-depth is achieved in 0.4 ms. These times are comparable with typical pulse times, so we cannot assume that the field is in local equilibrium. In the solid phase, the diffusion time is about twice as long.

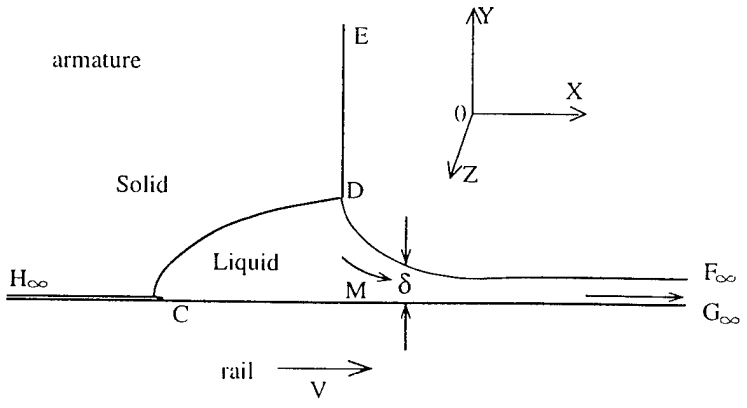

Figure 3: Armature-Rail interaction

2. Forces acting on the liquid phase

It is perhaps easier to understand the forces acting on the molten metal if we adopt a frame F that has the same velocity as F but no acceleration. In F the solid armature

is accelerating under the EM forces supplied by the current. If the liquid phase $\mathcal{L}$ is to 'keep up' with the solid armature, the forces acting on it must be sufficient to give it the same acceleration. But we cannot assume that the component of the magnetic pressure acting along the direction of travel has the same value on the free surface DF_∞ as on the solid boundary DE. It is more helpful to consider the force as being the usual volume distributed '$\mathbf{j} \times \mathbf{B}$' term that acts on a conductor, with the magnetic field $\mathbf{B}$ being due to the current $\mathbf{j}$.

Consider the case shown in Fig. 3. Suppose we adopt a two-dimensional approximation, with the magnetic field lying along OZ and the rail moving along the OX-axis in the positive direction. In this case

$$\frac{\partial B_z}{\partial x} = -\mu_0 j_y, \qquad \frac{\partial B_z}{\partial y} = \mu_0 j_x, \tag{4}$$

$$(\mathbf{j} \times \mathbf{B})_x = \quad j_y B_z = -\frac{\partial}{\partial x}\Big(\frac{1}{2\mu_0} B_z^2\Big). \tag{5}$$

and

$$(\mathbf{j} \times \mathbf{B})_y = -j_x B_z = -\frac{\partial}{\partial y}\Big(\frac{1}{2\mu_0} B_z^2\Big). \tag{6}$$

These equations give the EM forces acting on $\mathcal{L}$. There is one other force to consider, namely that due to the *gas* pressure. But this is such a very small fraction of the electromagnetic pressure, $B_z^2/2\mu_0$ that we can neglected it.

Evidently, because of friction, *some* of the liquid will adhere to the rail. As shown in Fig. 3, the thickness of this layer, δ say, determines the rate at which the melted armature material is removed from the 'pool' MCDM, where DM is a section at the original rear boundary of the armature. Let x denote the distance from the front edge of the liquid at C to M, then on the assumption that the boundary layer on CM is laminar, its displacement thickness a short distance downstream of DM is given by the classical expression[4]

$$\delta_1 = 1.72 \left(\frac{\nu x}{v}\right)^{1/2}, \tag{7}$$

where ν is the kinematic viscosity and v is the velocity of the free surface DF_∞ relative to the rail. This equation is based on the assumption that the depth above the layer is infinite, e.g. as in the flow past a flat plate. Later we shall verify that the thickness of the liquid pool is much greater than δ_1, which allows us to set $v = V$ (see Fig. 3). It follows that the mass flux per unit length of armature (in the OZ-direction) is given by

$$\text{Mass Flux} = \rho V \delta_1 = 1.72 \rho (\nu x V)^{1/2}. \tag{8}$$

In the case shown in Fig. 1, the current flowing through $\mathcal{L}$ is so small, that in the frame F there is only the friction force acting on the liquid, whereas the solid phase is accelerated away to the left by the EM forces acting on it. The liquid phase is confined to a narrow layer along CM, which simply 'wipes' the armature on to the rail as fast as the melting occurs.

3. Armature skin-depths

The equation determining the evolution of the magnetic field in an incompressible medium is[5]

$$\frac{\partial \mathbf{B}}{\partial t} + \mathbf{v}_e \cdot \boldsymbol{\nabla}\mathbf{B} = \mathbf{B} \cdot \boldsymbol{\nabla}\mathbf{v}_e + \xi \nabla^2 \mathbf{B}, \tag{9}$$

where $\mathbf{v}_e$ is the electron fluid velocity,

$$\mathbf{v}_e = \begin{cases} V\hat{\mathbf{x}} & -\mathbf{j}/en_e \quad \text{(rail)} \\ & -\mathbf{j}/en_e \quad \text{(armature)}\,. \end{cases} \tag{10}$$

in which $\hat{\mathbf{x}}$ is a unit vector parallel to the rails. Now

$$\boldsymbol{\nabla}\mathbf{B} = \left[\hat{\mathbf{x}}\frac{\partial}{\partial x} + \hat{\mathbf{y}}\frac{\partial}{\partial y}\right](B_z\hat{\mathbf{z}})\,,$$

so that from (4) we obtain

$$\mathbf{v}_e \cdot \boldsymbol{\nabla}\mathbf{B} = \begin{cases} -\mu_0 j_y V\hat{\mathbf{z}} & \text{(rail)} \\ 0 & \text{(armature)}\,. \end{cases}$$

Thus, since $\mathbf{B} \cdot \boldsymbol{\nabla} = 0$, in steady conditions (9) yields

$$\xi\left(\frac{\partial^2}{\partial x^2} + \frac{\partial^2}{\partial y^2}\right)B_z = \begin{cases} -\mu_0 j_y V & \text{(rail)} \\ 0 & \text{(armature)}\,. \end{cases}$$

We shall use superscripts 'r' and 'a' to denote rail and armature values. By (4) we can write the equations as

$$\xi_r\frac{\partial j_x^r}{\partial y} - \xi_r\frac{\partial j_y^r}{\partial x} + Vj_y^r = 0, \qquad \frac{\partial j_x^a}{\partial y} - \frac{\partial j_y^a}{\partial x} = 0\,. \tag{11}$$

It follows that the length scale for changes in j_y^r parallel to OX is $\delta_r = \xi_r/V$.

There are two rail/armature boundary conditions on $\mathbf{j}$. The first follows from the equation $\boldsymbol{\nabla}\cdot\mathbf{j} = 0$ integrated across the boundary, while the second follows from the $\hat{\mathbf{x}}$-component of Ohm's law, $\eta\mathbf{j} = \mathbf{E} + \mathbf{v}\times\mathbf{B}$, applied to each side of the interface, and the steady state equation $\boldsymbol{\nabla}\times\mathbf{E} = 0$ integrated across the boundary. These boundary conditions are:

$$\text{On } y = 0, \text{ for all } x: \qquad j_y^a = j_y^r\,, \qquad \eta_a j_x^a = \eta_r j_x^r\,. \tag{12}$$

Since j_y^a and j_y^r are the same at the interface, and δ_r is the x-length scale for j_y^r, it follows that at least just inside the armature, close to the rail δ_r is also the x-length scale for j_y^a. Within the armature

$$\frac{\partial j_x^a}{\partial x} + \frac{\partial j_y^a}{\partial y} = 0, \qquad \frac{\partial j_x^a}{\partial y} - \frac{\partial j_y^a}{\partial x} = 0\,, \tag{13}$$

and hence the scales for spatial changes in each current density component are determined entirely by the boundary conditions. The second of (13) shows that j_x^a has a y-length scale the same as the x-length scale of j_y^a, i.e. δ_r.

By $(12)_2$
$$\xi_r \frac{\partial^2 j_x^r}{\partial x \partial y} = \xi_r \frac{\partial}{\partial y}\left(\frac{\partial j_x^r}{\partial x}\right) = \xi_a \frac{\partial}{\partial y}\left(\frac{\partial j_x^a}{\partial x}\right),$$

where $\xi_a \equiv \eta_a/\mu_0$. Hence, differentiating $(11)_1$ by x, we get

$$\xi_a \frac{\partial}{\partial x}\left(\frac{\partial j_x^a}{\partial y}\right) - \xi_r \frac{\partial^2 j_y^a}{\partial x^2} + V\left(\frac{\partial j_x^a}{\partial y}\right) = 0.$$

on making use of $(12)_1$ and $(13)_2$. It follows that $\partial j_x^a/\partial y$ has a x-length scale of $\delta_a = \xi_a/V$. Therefore j_x^a has an x-length scale of δ_a. From $(13)_1$ the x-length scale of j_x^a is the same as the y-length scale of j_y^a.

Collecting these results, we have for the armature currents the following scales:

$$j_x: \quad x\uparrow = \delta_a,\ y\uparrow = \delta_r: \qquad j_y: \quad x\uparrow = \delta_r,\ y\uparrow = \delta_a,$$

with an obvious notation. We now identify the thickness of the melt wave with the y-length scale of the current density normal to the amature/rail interface, j_y^a (cf. Fig. 4). Thus

$$\mathsf{h} = \delta_a = \xi_a/V. \tag{14}$$

The current density normal to the rail/armature interface can now be expressed in the form

$$j_y = j_0 e^{x/\delta_r} e^{-y/\delta_a} \qquad (j_0 = \text{constant}). \tag{15}$$

The total current passing through the surface $y = 0$ is therefore

$$I = w\int_{-\infty}^{0} j_y\, dx = w\delta_r j_0, \tag{16}$$

where w is the depth of the surface of the armature in contact with the rail.

4. The Speed of the Melt-Wave

Let ρ, p, T denote the local density, pressure and temperature, c_v the specific heat at constant volume and $u = c_v T$ the specific internal energy. Also let $\boldsymbol{\pi}$ denote the viscous pressure tensor and v the fluid velocity, then $-\boldsymbol{\pi} : \boldsymbol{\nabla}\mathbf{v}$ is the viscous dissipation. We also need the heat flux vector, $\mathbf{q} = -\kappa\boldsymbol{\nabla}T$, the energy input per unit volume due to radiation, ψ, and the latent heat of melting, L_m. We shall assume that the melt-wave front is located at x_m, as shown in Fig. 4. With these definitions, the energy equation becomes[5]

$$\rho \mathrm{D}u + \rho p \mathrm{D}\rho^{-1} = -\boldsymbol{\pi} : \boldsymbol{\nabla}\mathbf{v} - \boldsymbol{\nabla}\cdot\mathbf{q} + \mathbf{j}\cdot(\mathbf{E} + \mathbf{v}\times\mathbf{B}) - \rho v_m L_m \delta(x_m) + \psi, \tag{17}$$

where $\delta(x_m)$ is the delta function, and

$$\mathrm{D} \equiv \frac{\partial}{\partial t} + \mathbf{v}\cdot\boldsymbol{\nabla}$$

is the convective time derivative.

For the solid phase, we replace the left-hand side by $\rho \mathrm{D}h - \mathrm{D}p \approx \rho \mathrm{D}h$, where h is the enthalpy, $c_p T$, and omit the viscous dissipation and radiation terms from the right-hand

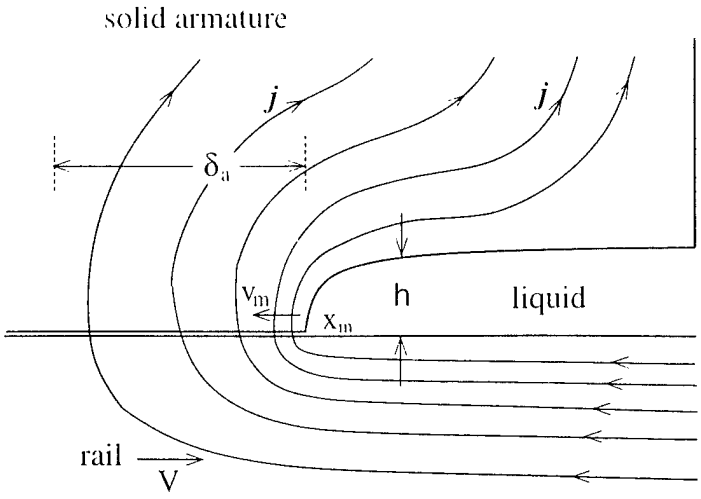

Figure 4: Resistive skin-depth in the armature

side. Then by Ohm's law,

$$\rho c_p \mathrm{D}T = \kappa \nabla^2 T + \eta j^2 - \rho L_m v_m \delta(x_m). \tag{18}$$

In order to simplify the theory, we now assume that in a frame fixed in the wave front, conditions are steady, which allows us to write $\mathrm{D}T = v_m\, dT/dx$ (see Fig. 4). Equation (18) now takes the form

$$\rho c_p v_m \frac{dT}{dx} = \kappa \left(\frac{d^2T}{dx^2} + \frac{d^2T}{dy^2} \right) + \eta j_0^2\, e^{2x/\delta_r}\, e^{-2y/\delta_a} - \rho L_m v_m \delta(0)\,. \tag{19}$$

We now integrate this equation over the length of the solid armature extending in front of the melt-wave, which we shall assume to be a relatively large distance. The second derivatives of the temperature vanish at $x = -\infty$ and the temperature gradient in the x-direction at the melt-wave front is zero. Thus, when (19) is integrated over $-\infty < x < 0$, the term containing $\kappa d^2T/dy^2$ vanishes. Next we integrate over $0 < y < \infty$. In the solid armature, close to the rail, we assume that $T(x, y)$ has the form

$$T = T_0 + (T_m - T_0)\, e^{x/\lambda}\, e^{-y/\lambda}\,,$$

where λ is the thermal skin depth. On using (16) and setting v_m zero outside the range $0 < y < \mathsf{h}$, after integration we arrive at

$$v_m = \frac{\overline{\eta}_a}{4\eta_r} \frac{\mu_0 I^2 V}{\rho Q w^2} - v_\kappa\,, \tag{20}$$

where $$v_\kappa \equiv \frac{\mu_0 \kappa}{\rho Q \overline{\eta}_a} (T_m - T_0) V\,, \qquad Q \equiv c_p (T_m - T_0) + L_m\,.$$

5. The Maximum Armature Speed

The acceleration of the armature projectile combination is given by the well-known formula

$$\frac{dV}{dt} = \frac{L'I^2}{2M} - \mathcal{F}. \tag{21}$$

where M is the total mass being accelerated. L' is the induction gradient and $\mathcal{F}$ is the sum of the various drag forces acting on the combination. Eliminating I between (20) and (21), we get

$$v_m = \frac{dx_m}{dt} = \frac{\overline{\eta}_a}{4\eta_r}\frac{\mu_0 M}{\rho Q w^2 L'}\left[\frac{dV^2}{dt} + 2V\mathcal{F}\right] - v_\kappa\,.$$

Let $x = a$ be the length of the armature in the OX-direction, then integrating over the time t_m that it takes the melt wave to travel this distance, we get

$$a = \frac{\overline{\eta}_a}{4\eta_r}\frac{\mu_0 M}{\rho Q w^2 L'}\left[V_c^2 - V_0^2 + 2\int_0^{t_m} V\mathcal{F}\,dt\right] - \int_0^{t_m} v_\kappa\,dt\,,$$

where V_0 is the speed of the armature at the instant that the melt wave is initiated and V_c is its speed when transition occurs. Hence

$$V_c^2 = \frac{4\eta_r}{\overline{\eta}_a}\frac{\rho Q w^2 L'}{M\mu_0}\left(a + \int_0^{t_m} v_\kappa\,dt\right) + V_0^2 - 2\int_0^{t_m} V\mathcal{F}\,dt. \tag{22}$$

Notice that friction decreases V_c, whereas heat loss to the rails, represented by the speed v_κ, increases V_c. As we shall show below, this heat loss is important: the adiabatic assumption adopted by some authors in rail-gun calculations is not justified.

6. Application of the Theory

We now return to the problem discussed in the Introduction. For the liquid model to be valid, we require that the rate at which the liquid metal is removed from the pool $MCDM$ (see Fig. 3) by boundary layer friction be less than the rate at which the volume of the pool is increased by melting. Thus, by (8) and (14) this condition is

$$\epsilon\delta_a v_m \geq \delta_1 V = 1.72(\nu x V)^{\frac{1}{2}}\,, \tag{23}$$

where ϵ is the fractional volume increase due to melting.

Suppose that the armature metal is Aluminium then we need the following physical values[6], all expressed in SI units:

Density: 2700 (25° C), 2640 (660° C; solid), 2410 (660° C; liquid).
Enthalpy of fusion 3.97×10^5, $c_p = 8.97 \times 10^2$, melting temperature $T_m = 660°$C.
Viscosity 1.38×10^{-3}, thermal conductivity 231,
resistivity 3.7×10^{-8} (25° C), 10.7×10^{-8} (660° C),

where the resistivity varies linearly with temperature. From these quantities we obtain

the three diffusivities:

$$\text{thermal}\quad \chi\ \ (\equiv \kappa_a/\rho c_p)\ = 1.07\times 10^{-4}, \qquad \text{viscous}\quad \nu = 5.7\times 10^{-7},$$

$$\text{resistive}\quad \xi_a\ \ (\equiv \eta_a/\mu_0) = 2.94\times 10^{-2}\ (25^{\circ}\,\mathrm{C}), \qquad \xi_a = 8.51\times 10^{-2}\ (660^{\circ}\,\mathrm{C}).$$

With Copper rails, we also require $\xi_r = 1.35\cdot 10^{-2}$ at 25° C.

For an Aluminium armature with Copper rails, we find from (7), (14) and (20) that

$$v_m = 5.16\times 10^{-16}(I/w)^2\,V - 9.9\times 10^{-4}V\,. \tag{24}$$

and
$$\mathsf{h} = \delta_a = 8.51\times 10^{-2}/V, \qquad \delta_1 = 1.3\times 10^{-3}(x/V)^{\frac{1}{2}}\,. \tag{25}$$

To illustrate the theory, we shall apply it to a rail-gun experiment carried out in the Institute for Advanced Technology[7]. Typical values are:

$w = a = 25\,\mathrm{mm}$, $I = 1.2\times 10^5\,\mathrm{A}$, $V = 600\,\mathrm{m/s}$, $dV/dt = 5\times 10^5\,\mathrm{m/s^2}$. In this case $v_m = 6.5\,\mathrm{m/s}$, $\mathsf{h} = 142\,\mu\mathrm{m}$, $\delta_1 = 8.4\,\mu\mathrm{m}$ at $x = 25\,\mathrm{mm}$. It would take the melt-wave a time $t_m = 3.8\,\mathrm{ms}$ to traverse the length a of the armature and initiate transition.

More accurately, the relation between a and t_m is

$$a = K_1\int_0^{t_m} I^2V\,dt - K_2\int_0^{t_m} V\,dt \qquad (K_1 = 5.16\times 10^{-16}/w^2,\quad K_2 = 9.9\times 10^{-4}). \tag{26}$$

Upon melting, the specific volume of Aluminium increases by the fraction $\epsilon = 0.088$. The melt-wave therefore increases the volume of the armature liquid per unit depth by $0.088\mathsf{h}v_m = 8.1\times 10^{-5}\,\mathrm{m^2/s}$. This is considerably less than the volume removed by friction, which from the left-hand side of (23) is $5.04\times 10^{-3}\,\mathrm{m^2/s}$. In this typical example, the inequality in (23) fails to be realised by two orders of magnitude. Evidently, the liquid model is not satisfactory. The liquid near the melt-wave front will flow towards the rail surface and will be removed faster than it can be replenished by expansion, with the result that a cavity will form near the interface and will extend along the inner surface of the liquid region. This is now the entrainment model and—according to the above theory—transition will occur as soon as the melt-wave reaches the front of the armature.

The critical velocity, i.e. the maximum attainable before transition, is given by (22). We shall ignore the friction force $\mathcal{F}$ and assume that the 'initial' velocity V_0 is zero. The value of L'/M follows from (21). First we shall omit the v_κ term. In this case (22) yields $V_c = 1.45\times 10^3\,\mathrm{m/s}$. From $V_c = t_m\,dV/dt$ we get $t_m = 2.9\,\mathrm{ms}$, which allows us to evaluate the omitted v_κ term. This increases V_c to $1.57\times 10^3\,\mathrm{m/s}$ and increases t_m to $3.1\,\mathrm{ms}$.

There is a very simple way of increasing V_c. Armatures that are 'spring-loaded' so that their surfaces are *always* pressed against the rails, regardless of the loss of width due to ohmic melting, would not allow the vapour phase and the consequent increase in the electrical resistance, to appear. There would be some additional friction loss at the beginning of the armature's motion relative to the rails, but this might be a price worth paying to avoid transition.

Finally, the reader should be reminded that the theory of this report and the conclusion just drawn, is based on a model that may not correctly represent the real physical situation.

Experimental evidence concerning the functional dependence of V_c is required at this stage. This should be compared with the dependence given by equation (22). Also the thickness and uniformity of the Aluminium deposited on the rails would be a useful guide to the nature of the melting process. To check the point made in the previous paragraph, one could vary the initial rail pressure on the armature by changing its size relative to the gap between the rails. If the theory is correct, this should alter the value of V_c.

7. Some other treatments

Parks[1] is concerned with developing a theory for the entrainment model. He gives an accurate description of the phenomenon, but fails to obtain correct values for the magnetic scale lengths. He assumes that the scale lengths are the same in the OX and OY directions (see his Fig. 1). His expression for h includes an additional factor η_a/η_r and consequently his formula for v_m is also incorrect, being $3.24(\eta_r/\eta_a)^2$ times the first right-hand term in (20)--he assumes that the process is adiabatic. The theory presented on the second page of his report has little relevance to the real problem, as the contradiction between his figures 1 and 2 immediately reveals. He even remarks at one stage that the presence of the gap between the armature and the rails will not appreciably alter the distribution of the current! Despite the 'rigorous' mathematical analysis, he ends up by adopting rough approximations that in effect reduce his approach to one of dimensional analysis, albeit wrong. His remarkable agreement with experiment is fortuitous.

James[2] litters his work with so many 'form factors', that it is not easy to read, but he does have a good grasp of the physics. However he has adopted the liquid model without justification.[1] Because he adopts the liquid model and allows the current to flow across it (see Fig. 2), James defines the current wave to be a vaporisation wave. To modify equation (20) to apply to this case, we need only to increase the value of Q to include the additional internal energy between the melting and vaporisation temperatures plus the heat of vaporisation. Apart from some form factors, James' formula for v_m is similar to that given by the first right-hand term in (20).

Barber and Challita[3] have no confidence in either the liquid or entrainment models, which they find irrelevant because the assumption of a perfect contact surface between rail and armature is never attained in practice. The electric current flows through discrete spots that occupy only a small fraction of the surface, and, they argue, this considerably weakens the influence of the velocity skin effect.

They consider the problem discussed above about the rates of production and loss of liquid and conclude that

> The mass rate of material removal [due to friction] is smaller than the mass rate of expansion at all velocities of interest. The ratio is about 30% at 1 km/s and increases with velocities to about 70% at 3 km/s. Therefore we do not expect a loss of lubrication and do not expect solid-solid friction to affect contact transition.

[1] About two years ago Trevor James asked me to help him find supporting arguments for this model. I considered only the forces acting on the liquid and decided, with making a serious calculation, that it was plausible. At that time I did not consider the competition between removal by friction and replacement by expansion, which I now think settles the case in favour of the entrainment model.

This conclusion appears to be in conflict with the one we deduced from (23). Their theory differs in detail, because they ignore the latent heat of melting, but the principle is the same. The two results are reconcilled when it is realised that the ratio of the right-hand side of (23) to the left-hand side depends on the dimension of the contact surface to the power 1.5. A typical spot has a radius of $100\,\mu$m. whereas the armature surface might be 10 mm or more across. It follows from these figures that in the spot model. the ratio just defined is about 10^{-3} smaller than in the liquid model. This is sufficient to satisfy the inequality corresponding to (23) and to justify the conclusion just quoted.

What remains to be considered is the extent to which the very high relative motion of the contact surfaces affects the spot model, which was originally developed for stationary surfaces. Experimental evidence for the model might be a streaked appearance of the Aluminum deposits on the rails. We shall give a detailed account of the spot model in another report.

References

1. Parks, P.B. *J. Appl. Phys.*, **67** (1), April 1990.
2. James, T.E. *7th EML Symposium*, San Diego, USA, April, 1994.
3. Barber, J.P. & Challita, A. *IEEE Trans. Magn.*, **29**, No. 1, 1993, 733–37.
4. Batchelor, G.K. *An Introduction to Fluid Dynamics*, CUP, 1967, p. 311.
5. Woods, L.C. *Kinetic Theory of Gases and Magnetoplasmas*, OUP, 1993, pp. 195–7.
6. Lide, D.R. (Ed.) *Handbook of Chemistry and Physics*. 76th ed. CRC Press, 1995.
7. Marshall, R.A., Persad, C., Jamison, K.A. & Matyac, M.J. *IEEE Trans. Magn.*, **31**, No. 1, 1995, 214–18.

Progress Report on Research into Electromagnetic Launchers

The Contact-Spot Model of Transition

December 1995

Professor L. C. Woods
University of Oxford
Mathematical Institute

The Contact-Spot Model of Transition

Summary

In Progress Report no. 1 (hereafter denoted by [1]), there is an account of the melt-wave model for transition in solid-armature, rail-gun launchers. This model contained a number of assumptions concerning the electrical, mechanical and thermal interactions between the rail and the armature. These are (i) perfect electrical contact, (ii) the removal of liquid metal by viscosity and (iii) adiabatic conditions except possibly in the region upstream of the melt-wave. As our main objective was to determine the speed of the melt-wave relative to the armature and to use this to calculate the projectile speed at which transition occurred, only the first of these assumptions was critical. However to determine the thickness of the material deposited on the rail by the passage of the armature, we made use of (ii) and (iii). We now believe that these are not good approximations, at least for the entrainment version of the melt-wave model and in §1 we shall change them. The modified theory will then be used to determine the thickness, δ_m, of the deposited layer.

In [1] we referred to the work of Barber and Challita[1] concerning the electrical contact between the armature and the rail. Their model of armature contact transition, first presented at the 5th EML Symposium[2], is based on 'adiabatic accumulation of resistive dissipation in contact spots'. Such spots are usually known as 'a-spots'[1]. In the melt-wave model, as shown in [1], the velocity skin effect (VSE) plays a central role in determining when transition occurs. However, with their model of electrical contact, Barber and Challita find that VSE has little effect on transition. Their treatment has some puzzling features, but their main point, namely that the melt-wave model is poor representation of the armature/rail interaction, is convincing. Our main task in this report is to develop a new theory for an 'a-spot', in thermal contact with its environment, and to use it to determine the thickness of deposited material and the time (of flight) at which we can expect transition to occur. The nature of the deposited layer enables us to decide between the melt-wave and a-spot models, since with the latter, we would expect to see a deposited layer of variable thickness, striated in the direction of motion. Some preliminary measurements of δ_m obtained at the Institute for Advanced Technology[3] show this feature.

1. The Entrainment Model Modified

In Figs. 1 and 2 we show the two versions of the melt-wave model that were considered in [1]. The liquid model is valid only if the rate at which the volume of the pool is increased by melting exceeds the rate at which it is removed by friction with the rail. In this case, it is reasonable to assume that the deposited thickness, δ_m, is approximately the same as the displacement thickness of the boundary layer that starts very close to the melt-wave front, where the fluid is relatively deep. However the condition on the rates is not met, so this model is not satisfactory. With the entrainment model, the fluid is never 'deep', so the boundary layer is not a relevant concept. In [1] we omitted to complete this model; we shall do that here.

A more important matter is the question of the thickness of the gap between the solid

[1] For the quaint reason that in the old literature on the subject, their radius was always denoted by the letter a!

armature and the rail behind the advancing melt-wave, denoted by h in Fig. 2. In §3 of [1], still adhering to an adiabatic description of the process, we argued that this should be equal to the y-length scale of the *current* density normal to the armature/rail interface just upstream of the melt-wave. Therefore, by the theory developed for this scale, we wrote

$$\mathsf{h} = \delta_a \qquad (\delta_a \equiv \xi_a/V, \quad \xi = \eta/\mu_0). \tag{1}$$

where V is the relative speed of the rail, η is the resistivity and ξ_a the magnetic diffusivity of the armature. One defect of this argument is that δ_a is the y-length scale for the current density in the same direction, i.e. of j_y, only close to the interface boundary and in front of the melt-wave. Since the components j_x and j_y satisfy Laplace's equation in the armature, their scale lengths are determined by the *nearest* boundary condition. Our argument inverts this—we have allowed the scale-length appropriate to one part of the boundary to determine the boundary condition for another part. The scale-length for j_y in the direction parallel to the wave-front, i.e. perpendicular to the interface, is to be determined from h, not the other way round. So what does determine h?

The adiabatic assumption is the problem, for it must be the *thermal* properties of the armature that will determine the range over which the heat from the intense electric current will extend. Of course if we were to adopt a mathematical approach and write down all the equations and boundary conditions, then no doubt the 'truth' of the matter would emerge automatically, but this would be a very difficult calculation, for behind the melt-wave, we have a moving boundary, whose location is initially unknown. Also we would need to include time in the list of independent variables, so increasing the dimensions to three—or four, if the true geometry of the armature is admitted. We shall avoid this complexity by adopting dimensional arguments, but avoiding empirical elements.

Let κ, ρ and c_p denote the thermal conductivity, density and specific heat at constant pressure of the armature material, then the thermal diffusivity is defined by $\chi = \kappa/\rho c_p$. This has the dimensions of a length squared over a time. Therefore, if t denotes the time during which the diffusion takes place, the distance of penetration of the heat is $(\chi t)^{\frac{1}{2}}$. This distance determines the width h. Hence (1) is replaced by

$$\mathsf{h} = (\chi t)^{\frac{1}{2}} \qquad (\chi \equiv \kappa/\rho c_p). \tag{2}$$

Let α denote the acceleration of the armature, then

$$\alpha = (kL'I^2 - F_a - F_d - F_p)/(m_a + m_p), \tag{3}$$

where m_a is the armature mass, m_p is the projectile mass, k is a constant, equal to $\frac{1}{2}$ or a little smaller, L' is the induction gradient of the gun, I is the total gun current, F_a is the ablation drag, F_d is the viscous drag and F_p is the retarding force due to the background gas. In a complete theory, we should use (3), but to obtain approximate results for the thickness of the layer on the rails, we shall be content to take α from experiment and also to give it a constant value; experiment indicates that this is roughly so over its middle range of values.

The assumption of constant acceleration allows us to write

$$V = \alpha t, \qquad x = \tfrac{1}{2}\alpha t^2, \qquad t = (2x/\alpha)^{\frac{1}{2}}, \tag{4}$$

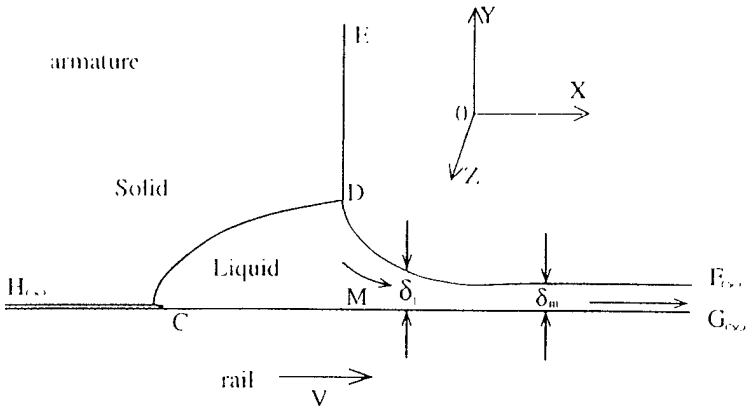

Figure 1: The Liquid Model

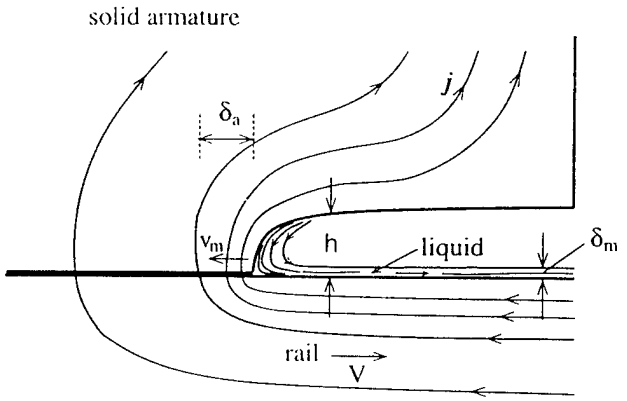

Figure 2: The Entrainment Model

where V is the armature velocity relative to the rails and x is its displacement at time t. We can now write (2) as

$$\mathsf{h} = \chi^{\frac{1}{2}} 2^{\frac{1}{4}} (x/\alpha)^{\frac{1}{4}} \qquad [\approx 4.63{\times}10^{-4} x^{\frac{1}{4}}], \tag{5}$$

where the numerical expression in (5) is for Aluminium, ($\chi = 1.07{\times}10^{-4}$), with the (experimental) average, $\alpha = 5{\times}10^{5}\,\mathrm{m\,s^{-2}}$. (We are not aiming at accuracy at this stage, but some rough estimates with which we can compare experiment.)

Now consider the conservation of mass in a frame fixed in the melt-wave front. With subscripts s and ℓ denoting the solid and liquid phases, and with v_m denoting the melt-wave velocity, on the assumption that the mass entrained on the rail equals the mass melted in the wave front, we get

$$\rho_s v_m \mathsf{h} = \rho_\ell (V + v_m)\delta_m .$$

Hence the thickness of the deposited layer is given by

$$\delta_m = \frac{\beta}{1+\beta}\frac{\rho_s}{\rho_\ell}\mathsf{h} \qquad (\beta \equiv v_m/V). \tag{6}$$

Equation (24) of [1] yields

$$\beta = v_m/V = 5.16\times(I/w)^2 \qquad [\approx 8\times10^{-13}I^2], \tag{7}$$

where w denotes the depth of the armature surface in contact with the rail and for the value in brackets, we adopted $w = 25.4\,\mathrm{mm}$. As $\beta \ll 1$, and $\rho_s/\rho_l = 2640/2419 = 1.095$, equations (5) to (7) yield

$$\delta_m = 8.76\times10^{-13}\, I^2\mathrm{h} = 4.05\times10^{-16}\, I^2 x^{\frac{1}{4}}\,. \tag{8}$$

For example, if $I = 3.5\times10^5\,\mathrm{A}$ and $x = 50\,\mathrm{mm}$, then $\mathrm{h} = 219\,\mu\mathrm{m}$ and $\delta_m = 23\,\mu\mathrm{m}$.

According to this theory, the deposition thickness is a maximum where $I^2x^{\frac{1}{4}}$ is a maximum, which will occur a very small distance beyond the station where the current is a maximum.

It is of interest to compare this with the boundary layer thickness, namely

$$\delta_1 = 1.72(\nu x/V)^{\frac{1}{2}} \quad \approx [4.11\times10^{-5}x^{\frac{1}{4}}]\,, \tag{9}$$

using the constant acceleration, $\alpha = 5\times10^5\,\mathrm{m\,s^{-2}}$. The thickness are similar for typical currents, $I \approx 3\times10^5\,\mathrm{A}$.

The characteristic width of the current layer just in front of the melt-wave is

$$\delta_r = \xi_r/V = \xi/(2x\alpha)^{\frac{1}{2}} \approx 1.35\times10^{-5}/x^{\frac{1}{2}}\,,$$

using the value of α given above. At $x = 50.8\,\mathrm{mm}$, this gives $60\,\mu\mathrm{m}$, a surprisingly narrow strip.

2. The Adiabatic Spot Model

On the melt-wave model, transition occurs when the melt-wave reaches the front of the armature. Here we shall consider the rather different description of transition proposed by Barber and Challita[2], based on the adiabatic accumulation of resistive dissipation in a-spots. Their first step was to use time-scale arguments to establish that there was insufficient time for heat to be lost from the spot by thermal conduction. We shall review this key phase of their argument.

We shall start with a general form for the energy equation in a fluid, with a fluid velocity v along OX, sheared in a direction along OY (see Fig. 1). Let ν denote the kinematic viscosity (or viscous diffusivity), then the viscous dissipation is $2\rho\nu(dv/dy)^2$; we also need the resistive dissipation, ηj^2, due to current density j, the heat flux vector, $\mathbf{q} = -\kappa\boldsymbol{\nabla}T$, and the latent heat of melting, L_m. In constant pressure changes the energy equation reads:

$$\rho c_p DT = \kappa\nabla^2 T + \eta j^2 + 2\rho\nu\left(\frac{dv}{dy}\right)^2 - \rho L_m v_m \delta(x_m)\,, \tag{10}$$

where

$$D \equiv \frac{\partial}{\partial t} + \mathbf{v}\cdot\boldsymbol{\nabla}$$

is the convective time derivative, $\delta(x_m)$ is the delta function, and v_m is the velocity of the melt-front at $x = x_m$.

To compare the terms, we define time scales τ_X by $\rho c_p \Delta T/\tau_X = X$, where X denotes a right-hand term in (10) and ΔT is a typical temperature change. Let a denote a characteristic length, such as the spot radius, and define the thermal diffusivity by $\chi = \kappa/\rho c_p$, then

$$\tau_\kappa = a^2/\chi\,, \quad \tau_\eta = \rho c_p \Delta T/(\eta j^2)\,, \quad \tau_\nu = c_p \Delta T \delta_1^2/(2\nu V^2)\,. \tag{11}$$

where for the viscous length scale, we have taken the boundary layer thickness defined in (9). To deal with the last term in (10), we integrate over a typical length and take $\tau_m^a = a/v_m$. We adopt the ohmic heating term for comparison. Thus

$$\tau_m^a = \rho L_m/(\eta j^2)\,, \tag{12}$$

gives the adiabatic melting time due to ohmic heating. We shall take ΔT to be the temperature increment required to raise the armature material to its melting point, then $\tau_\eta + \tau_m^a$ is the total time necessary to melt the material. We shall find it numerically convenient to replace j and a by $g = 10^{-10} j$, and $c = 10^4 a$. In SI units, we have

$$\chi = 1.07{\times}10^{-4}\,, \quad \rho = 2640\,, \quad \Delta T = 635\,, \quad c_p = 8.97{\times}10^2\,, \quad L_m = 3.97{\times}10^5\,,$$

$$\eta = 0.72{\times}10^{-7}\,, \quad \nu = 5.7{\times}10^{-7}\,, \quad j = 10^{10} g\,, \quad a = 10^{-4} c\,.$$

Using these values and (9), we arrive at the time scales

$$\tau_\kappa = 0.93{\times}10^{-4} c^2\,, \quad \tau_\eta = 1.90{\times}10^{-4}/g^2\,, \quad \tau_m^a = 1.46{\times}10^{-4}/g^2\,, \quad \tau_\nu = 8.44{\times}10^{-4} x^{-1/2}\,. \tag{13}$$

Evidently viscous heating is important only at large values of the displacement x. We shall ignore it in the following. With the values of I, w and δ_r given at the end of §1, we find $j_0 \approx 2{\times}10^{11}\,\mathrm{A\,m^{-2}}$, which suggested the factor 10^{10} in defining g. It remains to choose c and g.

The adiabatic assumption is valid only if $\tau_\kappa \gg \tau_\eta$, i.e. if $cg \gg 1.43$. In their first paper, Barber and Challita[2] accept the values $c = 10$ and $0.1 < g < 1$ as being typical; the adiabatic constraint is not satisfied at the lower currents. However in their second paper[1], they reduce c to 1 and have extended the range for g to 20. It follows that over the current range $0.1 < g < 1.43$, spots of this size are not adiabatic. In fact, at values of $a = 100\,\mu\mathrm{m}$ and $j = 10^{10}\,\mathrm{A m^{-2}}$, $\tau_\kappa < \tau_\eta$, which means that melting temperature cannot be reached. In the steady state ΔT is determined by $\tau_\kappa = \tau_\eta$, i.e. $\Delta T = \eta j^2 a^2/\kappa$.

It is reasonable to assume that, as with the entrainment model of Fig. 2, transition occurs when the material in physical contact at a point has completely melted. Using the adiabatic hypothesis, Barber and Challita[2] arrive at the empirical law,

$$k \int_{t_0}^{t_1} (I^2/F)\, dt = A \qquad (k = \text{const.}), \tag{14}$$

where t_0 is the conduction starting time, t_1 is the time of contact transition, A is the nominal contact area, F is the normal force on the contact and k is a constant, whose value depends only on the contact materials. Thus transition can be delayed by increasing

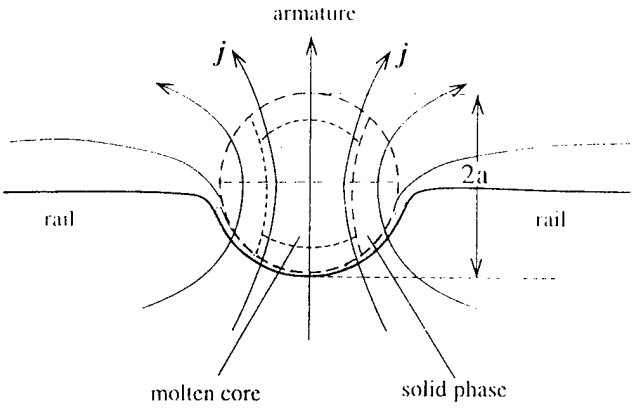

Figure 3: A Contact Spot

the contact force, increasing the contact area, or choosing a material with a low transition constant k. They found that the 'constant' k was not velocity dependent up to 1.2 km/s.

The first two of these conclusions are scarcely surprising and apply equally to a modified version of the melt-wave model. Evidently if there is a normal force on the contact, it will not be sufficient for the melt-wave to reach the front of the armature to initiate transition, for at this point, or perhaps a little earlier, the normal force will squeeze out the liquid between the surfaces and re-establish solid metal contact. This will continue until the normal force falls to a low value.

In their 1993 paper, Barber and Challita extended their work to greater speeds. They found that the transition 'constant' remained almost unchanged up to speeds of 2 km/s, allowing them to conclude that the velocity skin effect had little influence on the results, apart from shifting the current from leading spots to trailing spots.

3. The Diathermic Spot Model

We shall now develop a theory in which heat loses from the a-spot play a significant role in the phenomenon of contact currents. This is an extension of the classical treatment of the subject[3]. Fig. 3 illustrates an idealised contact spot. It is drawn on the assumption that the armature is the harder material, but this may be incorrect. However interchanging the rail and armature labels in the figure will have no effect on the theory to follow. As we have drawn it, initially an armature protuberance indents the rail, reaching pressures up to half of that necessary to make the indented material yield[3]. With copper, this is about 100 to 200 MPa. The intense flow of electric current through the restricted region of contact, heats it, completes the softening process and an a-spot is created. The central region quickly reaches the melting temperature and with continued ohmic heating, the liquid region spreads outwards. The relative motion of the rail and armature removes the molten metal as fast as it is created and when the spot is 'consumed' in this way, metallic contact between the rail and armature is lost *at this point*. As a-spots are 'burnt out', new spots will be able to form, as the surfaces come infinitesimally closer.

Initially the depth of indentation, a is determined by the hardness of the copper in the rail, but as the heating and softening rapidly proceeds, the thermal skin depth given by (5) will play a role. Which of these processes is dominant remains to be discovered; for our discussion, we shall adopt the thermal skin depth for the same reasons as advanced in §1.

In order to simplify the theory, we have modified the geometry of the spot shown in Fig. 3 to produce the axially symmetric representation shown in Fig. 4. The figure contains a central region of molten metal, expanding radially outwards with the progress of time. In drawing this figure, we have assumed that the copper rail is harder than the armature material. When the melt wave reaches the spot boundary at $r = a$, *local* transition will occur. But with a multitude of a-spots, potential and actual, this should not be confused with armature transition.

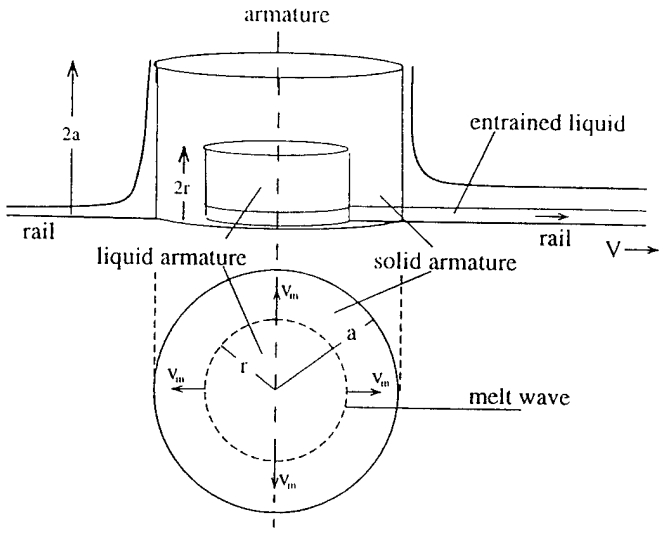

Figure 4: The Contact Spot Model

We shall first develop a theory for the stationary a-spot. We start from (10), omitting the unimportant viscous heating term. We integrate over the range $0 < t < \tau_0$, where τ_0 is the time at which the a-spot *first* reaches melting temperature. We cannot accurately represent the first right-hand term short of a full calculation, with appropriate boundary conditions. The sketch in Fig. 3, shows that this would be very dependent on the details of the spot geometry. We shall therefore be content with the approximation adopted in (11). Let

$$\langle \eta j^2 \rangle \equiv \frac{1}{\tau_0} \int_0^{\tau_0} \eta j^2 \, dt, \qquad \tau_\eta \equiv \frac{\rho c_p \Delta T}{\langle \eta j^2 \rangle}, \tag{15}$$

then (10) yields $\tau_0^{-1} = \tau_\eta^{-1} - \tau_\kappa^{-1}$, i.e.

$$\tau_0 = \frac{\tau_\eta \tau_\kappa}{\tau_\kappa - \tau_\eta} \qquad (\tau_\kappa > \tau_\eta). \tag{16}$$

Adopting the constant values of η and j used in (13), this gives

$$\tau_0 \approx \frac{1.09 \times 10^{-4} c^2}{(cq)^2 - 2.01} \qquad (cq > 1.43). \tag{17}$$

When the melting temperature has been achieved, the spot remains at constant temperature during the passage of a melt wave from the axis to the spot boundary. For this case (10) yields

$$\rho c_p v_m \frac{dT}{dr} = \frac{\kappa}{r}\frac{d}{dr} r \frac{dT}{dr} + \eta j^2 - \rho L_m v_m(r)\delta(r).$$

We shall assume that the cylindrical contact region is all at the melting temperature, so that the left-hand term is zero. Multiplying by $2\pi r$ and integrating over $0 < r < a$, we find

$$v_m = (a^2\eta j^2 - \kappa\Delta T)/(2\rho L_m r). \tag{18}$$

where we have written $[dT/dr]_{r=a}$ as $-\Delta T/a$.

The time required to melt the whole of the cylinder is $\tau_m = \int_0^a dr/v_m$. Hence, using (11) and (12), we obtain

$$\frac{1}{\tau_m} = \frac{1}{\tau_m^a} - \Big(\frac{2c_p\Delta T}{L_m}\Big)\frac{1}{\tau_\kappa}. \tag{19}$$

Adding τ_0 and τ_m, we arrive at the time for spot transition, $\tau_{\rm tr}^s$:

$$\tau_{\rm tr}^s = \frac{\tau_\eta\tau_\kappa}{\tau_\kappa - \tau_\eta} + \frac{\tau_m^a\tau_\kappa}{\tau_\kappa - 2.87\tau_m^a}, \tag{20}$$

on using the numerical values given in §2. Hence from (13),

$$\tau_{\rm tr}^s = 10^{-4}c^2\left\{\frac{1.90}{(cg)^2 - 2.04} + \frac{1.46}{(cg)^2 - 4.51}\right\} \qquad (cg > 2.12). \tag{21}$$

A typical value, with $c = 1.5$ and $g = 5$, is $\tau_{\rm tr}^s = 14\,\mu$s.

4. Modification Due to the Velocity Skin Effect

It is obvious from Fig. 3 that rapid relative motion between the armature and rail will render the above theory irrelevant. For example at $V = 500\,\mathrm{m\,s^{-1}}$, the diameter of the example at the end of the previous section, $2a = 3{\times}10^{-4}$ m, will be traversed in $0.6\,\mu$s, long before the melting temperature is achieved.

The velocity skin effect will cause a concentration of the electric current near the rear of a sliding contact spot. The heating will not be symmetric, as depicted in Fig. 3, but will result in a melt wave, that passes through the spot with a velocity v_m, as illustrated in Fig. 5. Equation (20) of [1], viz.

$$v_m = \frac{\bar\eta_a}{4\eta_r}\frac{\mu_0 I^2 V}{\rho Q w^2} \qquad (Q = c_p(T_m - T_0) + L_m,\ I = \delta_r w j_0,\ \delta_r = \eta_r/\mu_0 V),$$

will apply. Hence

$$v_m = \Big(\frac{\bar\eta_a\eta_r}{4\rho Q\mu_0}\Big)\frac{j_0^2}{V} \approx 9.53\frac{g_0^2}{V} \qquad (g_0 = 10^{-20} j_0). \tag{22}$$

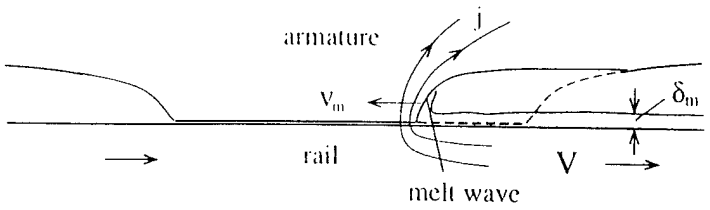

Figure 5: A Melt Wave Crossing an A-Spot

The spot transit time is therefore

$$\tau_s = 0.105\frac{2aV}{g_0^2}. \tag{23}$$

The thickness δ_m of the deposited layer is given by (6), modified for the present application. From (4) to (6),

$$\beta = v_m/V = 9.53(g_0/V)^2, \quad \mathrm{h} = 1.23{\times}10^{-2}(x/\alpha)^{\frac{1}{4}}, \quad V = (2\alpha x)^{\frac{1}{2}}. \tag{24}$$

Hence
$$\delta_m = \beta(\rho_s/\rho_\ell)\mathrm{h} = 6.42{\times}10^{-2}\frac{g_0^2}{\alpha^{\frac{5}{4}}x^{\frac{3}{4}}}. \tag{25}$$

There remains the difficult question of defining transition for the armature as a whole. The velocity skin effect will concentrate the current into the a-spots closest to the rear edge of the armature face in contact with the rail. To facilitate the description, imagine these to be in rows parallel to the trailing edge. As each row of spots is eliminated, the current will move forward to the spots in the next row, and so on until the front row is reached. Of course it may not happen in this way—new spots might appear behind the rows already visited. But let us assume that row by row elimination is a rough approximation to the process.

There is one important variable that is particularly difficult to determine. This is the ratio ε of conducting area in the spots to the actual area of the armature face, or equivalently, the number density $N_s = \varepsilon/(\pi a^2)$ of spots of radius a. Values of ε of between 0.1 and 0.2 have been quoted[2]. If we rearrange the circles into squares of the same area, we find that the conducting length per unit length of armature is $\varepsilon^{\frac{1}{2}}$. Then if w is the width of the armature measured parallel to the rails, the conducting length is $w\varepsilon^{\frac{1}{2}}$, and the transition time for the armature is τ_a, where

$$\tau_a = w\varepsilon^{\frac{1}{2}}/v_m = 0.105w\varepsilon^{\frac{1}{2}}V/g_0^2. \tag{26}$$

To illustrate the theory with some numbers, let us assume that $\alpha = 5{\times}10^5\,\mathrm{m\,s^{-2}}$, $g_0 = 10$, $a = 1.5{\times}10^{-4}\,\mathrm{m}$, $w = 0.025\,\mathrm{m}$, $w = 0.05\,\mathrm{m}$, $\varepsilon = 0.1$. Then from (23) to (26) we get

$$\tau_s = 71\,\mu\mathrm{s},\ V = 224\,\mathrm{m\,s^{-1}},\ v_m = 4.25\,\mathrm{m\,s^{-1}},\ \mathrm{h} = 218\,\mu\mathrm{m},\ \delta_m = 5\,\mu\mathrm{m},\ \tau_a = 1.86\,\mathrm{ms}.$$

The next stage in the research requires some experimental data to allow us to confirm or reject the above theory. Examination of the surfaces of the armature and the rail after rail-gun firings should provide valuable clues. However, even if the theory is correct so far as the thermal effects are concerned, *transition* may have a different cause.

The elastic properties of the armature/rail system need to be considered. The lateral force on the rails by the magnetic field is a load that moves with the velocity V of the armature. It is known[4] that moving loads on elastically supported beams can excite disturbances in the beam and more important, that there is a critical velocity V^* at which the energy does not radiate away from the moving load, but builds up in its vicinity. In the absence of damping, the response becomes infinite as V approaches V^*. The value of this critical velocity is

$$V^* = \left(\frac{4kEI}{\rho^2 A^2}\right)^{\frac{1}{4}} , \tag{27}$$

where E is Young's modulus, I is the moment of inertia, ρ is the density, A is the cross-section area and k is the restoring force per unit displacement of the beam in the lateral direction. When V reaches V^*, the displacement of the rail may be sufficient to break the contact between the armature and rail and cause transition. Research on this possibility will be reported later.

References

1. Barber, J.P. & Challita, A. *IEEE Trans. Magn.*, **29**, No. 1, 1993, 733–37.
2. Barber, J.P., Challita, A. Maas, B. & Thurmond, L. *IEEE Trans. Magn.*, **27**, No. 1, 1991, 228–232.
3. Holm, R., *Electrical Contacts*, Almqvist & Wiksells, Uppsala, 1946.
4. Graff, K.F. *Wave Motion in Elastic Solids*, Clarendon Press, Oxford, 1975, p. 175.

Progress Report on Research into Electromagnetic Launchers

8th EML Symposium Paper:

The Current Melt-Wave Model

January 1996

Professor L. C. Woods
University of Oxford
Mathematical Institute

8th EML Symposium Paper: The Current Melt-Wave Model

Comments on the Paper

This report embodies the paper that I am submitting to the 8th EML Symposium to be held in April in Baltimore. It is attached below and may undergo minor revisions before presentation. It is based on the theory presented in my first Progress Report, which gave an account of a melt-wave model for transition in solid-armature, rail-gun launchers. This report contained a number of assumptions concerning the electrical, mechanical and thermal interactions between the rail and the armature. These were (i) perfect electrical contact, (ii) the removal of liquid metal by viscosity, (iii) in addition to the (obvious) boundary condition, $j_y^r = j_y^a$, on the normal component of the current density, a boundary condition on the *transverse* current density at the armature/rail interface of the form $\eta_r j_x^r = \eta_a j_x^a$, where the subscripts 'a' and 'r' denote armature and rail and η is the resistivity, (iv) adiabatic conditions except possibly in the region upstream of the melt-wave, (v) that the width of the gap, h between the armature and the rail is based on an *electrical* scale-length and (vi) (dependent on (iii)) that this scale length is $\delta_a \equiv \eta_a/(\mu_0 V)$.

In preparing the EML paper, I decided to replace the dimensional arguments used to obtain (vi) by a mathematical solution of the equations satisfied by the current density. The dimensional argument was based on the two boundary conditions in (iii), which lead naturally to two distinct length scales for change in the currents within the armature, namely δ_r and δ_a. The thickness h was then identified with the length scale of the normal current, j_y^a in the OY-direction, which proved to be δ_a. But this is not support by the mathematical solution, which shows that there can be only *one* length scale within the armature (see equation (9) below). This length scale is that imposed on the armature currents by an outer boundary condition in the rail; it is therefore δ_r, not δ_a. The basic error in the first report was to follow Parks [3] and adopt the second boundary condition in (iii).

The second boundary condition followed from the transverse component of Ohm's law, $\eta\mathbf{j} = \mathbf{E} + \mathbf{v}\times\mathbf{B}$, applied to each side of the interface, and the steady state equation $\nabla\times\mathbf{E} = 0$, integrated across the boundary, which reputedly shows that the transverse component of the electrical field is continuous. At first sight this is plausible, but it is not valid for a reason I gave in my book, *Principles of Magnetoplasma Dynamics*, OUP, 1987, (pp. 116–17) and had overlooked. Boundary conditions are obtained by applying transition rules to the field equations and then applying physical conditions for setting surface intensities equal to zero. By surface intensities is meant delta function infinities in the property in question, a familiar example being the current sheet $\mathbf{j}^*$ appearing in the transition rule $\mathbf{n}\times[\mathbf{B}] = \mu_0\mathbf{j}^*$, obtained by integrating $\nabla\times\mathbf{B} = \mu_0\mathbf{j}$ across a surface with unit normal $\mathbf{n}$. Only if we can adduce physical reasons for $\mathbf{j}^*$ being zero, such as a significant resistivity, can we infer the boundary condition $\mathbf{n}\times[\mathbf{B}] = 0$. Otherwise the condition merely gives us a means of determining the strength of the current sheet—it is not a boundary condition.

When the field equation $\nabla\times\mathbf{E} = 0$ is integrated across a surface layer, the result is

$$\mathbf{n}\times[\mathbf{E}] + \nabla_{\|}\times\mathbf{E}^* = 0,$$

where $\nabla_{\|}$ is an gradient operator lying in the surface and $\mathbf{E}^*$ is an electric field surface intensity. The physical origin of $\mathbf{E}^*$ is an electric dipole layer of strength τ^* say, which gives $\mathbf{E}^* = \mathbf{n}\tau^*$. If the length scale of interest in the physical problem, $\mathcal{L}$ say, is greater

than a Debye length, it is not possible to set τ^* equal to zero. The Debye length is very small on an MHD scale of length so in rail-gun physics we cannot set $\mathbf{E}^*$ equal to zero, which in turn means that we are unable to assume that $\mathbf{n}\times[\mathbf{E}] = 0$. It is therefore not true that $\eta_a j_x^a = \eta_r j_x^r$ and therefore the paper has only one length scale for the armature current, namely δ_r.

In my second report (*The Contact-Spot Model of Transition*) it was explained that the liquid model—i.e. the model in which most of the melted metal remained filling the gap—is valid only if the rate at which the volume of the pool is increased by melting exceeds the rate at which it is removed in a boundary layer by friction with the rail. The model was rejected since the condition on the rates is not met. With the entrainment model, the fluid is never 'deep', so the 'boundary layer' is not a relevant concept. It seems very reasonable to expect that, as fast as the melt is created by ohmic heating, it will be removed simply by adherence on the rail. As shown at the end of the attached EML paper, this model gives a thickness δ_m of solidified Aluminum on the rail of about $20\,\mu$m, a value that is supported by measurements. I have included one other important change at this point—I have allowed for pressure between the armature and rail by admitting repeated traverses of the armature by the melt wave. Transition is defined as occurring when removal of the armature surface reduces the pressure to zero.

Returning to the list in the first paragraph above, I have removed the adiabatic assumption of (iv), a change that generates the 'G' term in equations (18) and (20) of the paper below. It proves to be only a small correction in (18), but more significant in the expression (20) for the velocity of the armature at transition.

A more important matter is the question of what process determines the thickness, h, of the gap between the solid armature and the rail behind the advancing melt-wave. In my first report I adopted (v), i.e. accepted an electrical scale length for h, but in my second report (mainly concerned with the nature of the electrical contact) I changed to a thermal scale length by an uncertain argument that no longer convinces me. It may be correct, but in the EML paper, I have thought it prudent to return to the electrical scale length. Supporting this, there is the fact that the time-scale for electrical changes over a given length, being inversely proportional to the magnetic diffusivity, is much smaller that the time scale for thermal changes over the same distance. I expect to return to this question in later reports.

The Current Melt-Wave Model

L. C. Woods

Institute for Advanced Technology, University of Texas at Austin
& Mathematical Institute, University of Oxford

Abstract—It is generally accepted that the velocity skin effect concentrates the current crossing the armature/rail interface at the rear corners of a solid armature. Ohmic heating melts these corners and the molten metal is removed by being entrained on the rail. As the resistivity of the resulting gap exceeds that of the solid phase, the current is deflected forwards into the solid region. The mechanism results in a 'melt-wave' moving from the back to the front of the armature, leaving a high resistance plasma gap of width h, between the armature and the rails. Transition to a high contact voltage is therefore a likely outcome when the melt wave reaches the front of the armature, although if the armature is compressed by the rails, several successive meltings along the armature surface will be required to reach transition. In this paper we give a theory for the speed v_m at which the melt wave advances relative to the armature. Our model differs from those proposed by other authors in that h depends only on the electrical skin depth in the rail and since $v_m \propto \mathsf{h}^{-1}$, our value for v_m is different. An expression for the armature speed V_c at which transition can occur is also derived.

1. INTRODUCTION

The main assumptions on which our model depends are (i) perfect electrical contact between the armature and rail ahead of the melt wave and (ii) the rapid removal of the liquid metal by entrainment on the rail. The first assumption is not very satisfactory, since the electric current is actually transported across the gap between rail and armature through small contact spots [1] [2], but the model will at least serve to establish an ideal value for the time to transition. Also, if the pressure between the surfaces is 'large', the spots will increase in size and number under this normal force and the electrical contact will begin to resemble the ideal case.

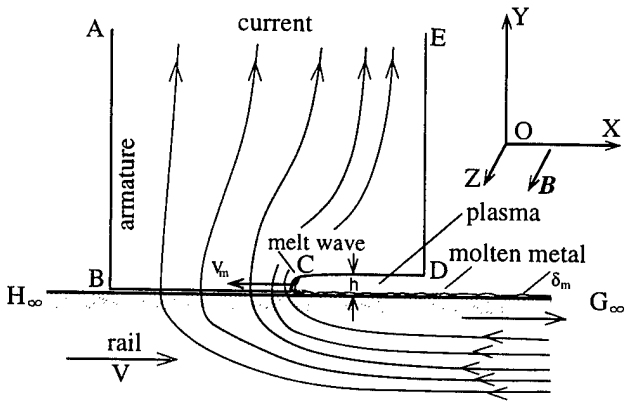

Figure 1: Melt-wave model

The melt-wave model is illustrated in Fig. 1. The wave is advancing with a speed v_m relative to the armature, moving from D to B, and when it reaches B, provided the gap h remains large enough not to be suppressed by the normal pressure between the surfaces, transition will result.

An expression for v_m can be deduced from the energy equation applied to the solid region of the armature extending in front of the melt wave. We shall show that it is given by

$$v_m = \frac{\alpha\overline{\eta}_a\mu_0 I^2 V}{2\eta_r\rho Q w^2} - \frac{2\alpha\mu_0 GV}{\pi\eta_r}, \qquad \left(\mathsf{h} = \frac{\pi\eta_r}{2\alpha\mu_0 V},\ \alpha \approx 1.148\right), \tag{1}$$

where $$Q \equiv c_p(T_m - T_0) + L_m, \qquad G \equiv \frac{c_p(T_m - T_0)}{Q}\chi_a\left[1 + \left(\frac{\chi_a}{\chi_r}\right)^{\frac{1}{2}}\right], \tag{2}$$

and for completeness, we have included the expression for h. In these expressions $\overline{\eta}_a$ is an average resistivity in the solid armature, η_r is the rail resistivity, I is the total current flowing through the armature, μ_0 is the permeability of free space, ρ is the armature density, w is the depth of the surface of the armature in contact with a rail, T_m is the melting temperature, T_0 is the laboratory temperature, L_m is the enthalpy of fusion (latent heat), c_p is the specific heat at constant pressure, χ_a, χ_r are the thermal diffusivities in the armature and rail and V is the speed of the armature. The armature speed V_c at which transition occurs is given in equation (20).

While Parks [3] gives an accurate description of the phenomenon, he obtains values for the scale length for changes in the magnetic field that appear to be in error. His expression for the melt-wave gap, h, includes an additional factor $0.45(\eta_a/\eta_r)^2$, and since $v_m \propto \mathsf{h}^{-1}$, his formula for v_m disagrees with ours. Also the conflict between his figures 1 and 2 is puzzling, as is his remark that the presence of the gap between the armature and the rails will not appreciably alter the distribution of the current.

James [4] adopts a model in which the melted metal from the armature is only slowly removed by the rail. It therefore fills the gap between the armature and rail, which allows some current to flow across the gap. To some extent this weakens the melting process and it also means that melting alone is not sufficient to yield transition. James therefore defines the current wave to be a vaporisation wave. To modify equation (1) to apply to this case, we need to increase the value of Q to include the additional internal energy between the melting and vaporisation temperatures plus the heat of vaporisation.

Barber and Challita [2] have no confidence in melt-wave models, which they find irrelevant because the assumption of a perfect contact surface between rail and armature is never attained in practice. The electric current flows through discrete spots that occupy only a small fraction of the surface, and, they argue, this considerably weakens the influence of the velocity skin effect. Their treatment of armature contact transition, is based on 'adiabatic accumulation of resistive dissipation in contact spots'. Whether the contact spots are really adiabatic depends very much on their size, which is poorly known. We agree with some features of their model. Ours is an idealized description with which to compare experiments and more physical representations of electrical contact.

2. THE CURRENT DENSITY

We shall adopt a two-dimensional model, as depicted in Fig. 1, with axes fixed in the armature. The magnetic field $\mathbf{B}$ is directed along OZ, the rails move parallel to OX with speed V and the electric current $\mathbf{j}$ lies in the (X,Y)-plane. Unit vectors along the axes are denoted by $\hat{\mathbf{x}}$, $\hat{\mathbf{y}}$, $\hat{\mathbf{z}}$. The equation determining the evolution of the magnetic field in an incompressible medium is [5]

$$\frac{\partial \mathbf{B}}{\partial t} + \mathbf{v}_e \cdot \boldsymbol{\nabla}\mathbf{B} = \mathbf{B} \cdot \boldsymbol{\nabla}\mathbf{v}_e + \xi \nabla^2 \mathbf{B}, \tag{3}$$

where $\xi \equiv \eta/\mu_0$ is the magnetic diffusivity and $\mathbf{v}_e$ is the electron fluid velocity,

$$\mathbf{v}_e = \begin{cases} V\hat{\mathbf{x}} & -\mathbf{j}/en_e \quad \text{(rail)} \\ & -\mathbf{j}/en_e \quad \text{(armature)}\,, \end{cases} \tag{4}$$

in which en_e is the electron charge density.

With the relations

$$\frac{\partial B_z}{\partial x} = -\mu_0 j_y, \qquad \frac{\partial B_z}{\partial y} = \mu_0 j_x\,, \tag{5}$$

we obtain

$$\mathbf{v}_e \cdot \boldsymbol{\nabla}\mathbf{B} = \begin{cases} -\mu_0 j_y V \hat{\mathbf{z}} & \text{(rail)} \\ 0\,\hat{\mathbf{z}} & \text{(armature)}\,. \end{cases}$$

We shall assume that in a frame fixed in the melt-wave front, the thermal and electric fields are in a quasi-steady state, by which we mean that on a time scale short compared with the transit time of either the armature from breech to muzzle or the melt wave through the armature, the fields will appear static. This approximation will evidently fail near either end of these transits. In a typical experiment at IAT, Austin, we find that the diffusion time for the electric field through a $\frac{1}{4}$ inch copper rail is about 1 ms, which is not much less than the armature transit time. So a genuine steady state in the electric field is never attained.

Since $\mathbf{B} \cdot \boldsymbol{\nabla} = 0$, in steady conditions (3) yields

$$\xi \left(\frac{\partial^2}{\partial x^2} + \frac{\partial^2}{\partial y^2} \right) B_z = \begin{cases} -\mu_0 j_y V & \text{(rail)} \\ 0 & \text{(armature)}\,. \end{cases}$$

We shall use superscripts 'r' and 'a' to denote rail and armature values. By (5) we can write the equations as

$$\xi_r \frac{\partial j_x^r}{\partial y} - \xi_r \frac{\partial j_y^r}{\partial x} + V j_y^r = 0, \qquad \frac{\partial j_x^a}{\partial y} - \frac{\partial j_y^a}{\partial x} = 0\,. \tag{6}$$

We also have $\boldsymbol{\nabla} \cdot \mathbf{j} = 0$ in both domains, i.e.

$$\frac{\partial j_x^r}{\partial x} + \frac{\partial j_y^r}{\partial y} = 0, \qquad \frac{\partial j_x^a}{\partial x} + \frac{\partial j_y^a}{\partial y} = 0\,. \tag{7}$$

Eliminating j_x^r from $(6)_1$ and $(7)_1$, we get

$$\delta_r^2 \frac{\partial^2 j_y^r}{\partial y^2} + \delta_r \frac{\partial}{\partial x}\Big\{\delta_r \frac{\partial j_y^r}{\partial x} - j_y^r\Big\} = 0\,, \tag{8}$$

where $\delta_r \equiv \xi_r/V$. Notice that with $x' = x/\delta_r$, $y' = y/\delta_r$, the equation takes a dimensionless form.

We now assume that the wave front lies on $x = 0$ and that the rail/armature interface lies on $y = 0$. As we are interested in a solution near the origin, the geometry suggests that we solve (8) by a separation of variables, i.e. by writing $j_y^r = X(x)Y(y)$. We require j_y^r to vanish at $x = \infty$. The solution is therefore the sum over the separation parameter m of terms of the the type

$$j_y^r = A_m \cos(my/\delta_r) e^{\alpha x/\delta_r}\,, \qquad \alpha = \tfrac{1}{2}\{(1+4m^2)^{\frac{1}{2}} - 1\} \qquad (x < 0,\, y < 0). \tag{9}$$

To determine m we consider the diffusion of the electric field into the rail as viewed from the armature. In a time interval δt, a current element diffuses a short distance $y = -(\xi_r \delta t)^{\frac{1}{2}}$ into the rail as it is convected a distance $x = V\delta t$ along OX. The element therefore moves at a small angle $\theta = (\xi_r \delta t)^{\frac{1}{2}}/(V\delta t)$ to OX. Hence its displacement along OY, as seen from the armature, is $\theta(\xi_r \delta t)^{\frac{1}{2}} = \xi_r/V = \delta_r$. It follows that j_y^r must fall to zero at $y = -\delta_r$. Hence by (9), $m = \pi/2$ and $\alpha = \frac{1}{2}\{(1+\pi^2)^{\frac{1}{2}} - 1\} \approx 1.148$.

On integrating $\boldsymbol{\nabla} \cdot \mathbf{j} = 0$ across the interface $y = 0$, we obtain the boundary condition $j_y^a(x,\,0) = j_y^r(x,\,0)$, whence from (9)

$$j_y^a(x,\,0) = j_0 e^{\alpha x/\delta_r} \qquad (-\infty < x < 0), \tag{10}$$

where j_0 is the current density at the origin. The appropriate continuation of this boundary value into the armature is

$$\begin{matrix} j_x^a(x,\,y) \\ j_y^a(x,\,y) \end{matrix} = \begin{matrix} \sin(\alpha y/\delta_r) \\ \cos(\alpha y/\delta_r) \end{matrix} j_0 e^{\alpha x/\delta_r} \qquad (-\infty < x < 0,\; 0 < y < \mathsf{h}), \tag{11}$$

which satisfies $(6)_2$ and $(7)_2$. We chose h to be the distance at which the current flowing into the armature first falls to zero, i.e. where $\alpha \mathsf{h}/\delta_r = \pi/2$. Hence

$$\mathsf{h} = \frac{\pi \delta_r}{2\alpha} \approx 1.368\,\delta_r = \tfrac{1}{2}\pi\ell, \qquad (\ell \equiv \delta_r/\alpha)\,. \tag{12}$$

From (11)

$$j_y^a(x,\,0) = j_0 e^{x/\ell}, \qquad j^2(x,y) = j_0^2 e^{2x/\ell}\,, \tag{13}$$

where j is the armature current density. The total current passing through the surface $y = 0$ is therefore

$$I = w \int_{-\infty}^{0} j_y\, dx = w\ell j_0, \tag{14}$$

where w is the depth of the surface of the armature in contact with the rail.

3. THE SPEED OF THE MELT WAVE

We start with the energy equation

$$\rho c_p \mathrm{D}T = \kappa \nabla^2 T + \eta j^2 - \rho L_m v_m \delta(x_m), \tag{15}$$

where $D \equiv \partial/\partial t + \mathbf{v}\cdot\boldsymbol{\nabla}$ is the convective time derivative, κ is the thermal conductivity, $\delta(x_m)$ is the delta function and the other variables have been defined in the Introduction. Our assumption that, in a frame fixed in the wave front, conditions are steady, allows us to write $\mathrm{D}T = v_m\,\partial T/\partial x$. Equation (15) now takes the form

$$\rho c_p v_m \frac{\partial T}{\partial x} = \kappa_a \left(\frac{\partial^2 T}{\partial x^2} + \frac{\partial^2 T}{\partial y^2} \right) + \eta_a j_0^2 e^{2x/\ell} - \rho L_m v_m \delta(0)\,. \tag{16}$$

This equation is next integrated over $-\infty < x < 0$ and $0 < y < \mathsf{h}$. As $\partial T/\partial x$ is zero at $x = 0$ and $x = -\infty$, the thermal conductivity term yields

$$\int_{-\infty}^{0} \kappa_a \left[\frac{\partial T}{\partial y}\right]_0^{\mathsf{h}} dx \approx -\kappa_a(\lambda_a^{-1} + \lambda_r^{-1}) \int_{-\infty}^{0} (T - T_0)\, dx \approx -\kappa_a(1 + \lambda_a/\lambda_r)(T_m - T_0),$$

where λ_a, λ_r are the thermal skin depths, $(\chi_a t_0)^{\frac{1}{2}}$ and $(\chi_r t_0)^{\frac{1}{2}}$. With the help of (12) through (14), the integrated equation yields the solution given in (1) and (2), viz.

$$v_m = \frac{\alpha\overline{\eta}_a \mu_0 I^2 V}{2\eta_r \rho Q w^2} - \frac{2\alpha\mu_0 G V}{\pi\eta_r}\,, \qquad \left(\mathsf{h} = \frac{\pi\eta_r}{2\alpha\mu_0 V},\ \alpha \approx 1.148\right), \tag{17}$$

where $$Q \equiv c_p(T_m - T_0) + L_m\,, \qquad G \equiv \frac{c_p(T_m - T_0)}{Q}\chi_a\left[1 + \left(\frac{\chi_a}{\chi_r}\right)^{\frac{1}{2}}\right]. \tag{18}$$

The acceleration of the armature/projectile combination is given by the well-known formula

$$\frac{dV}{dt} = \frac{L' I^2}{2M} - \mathcal{F}, \tag{19}$$

where M is the total mass being accelerated, L' is the induction gradient and $\mathcal{F}$ is the sum of the various drag forces acting on the combination. We shall assume that the armature is under pressure from the rails and that until a width $f\mathsf{h}$ is removed from each side of the armature, electrical contact is maintained. Eliminating I between (17) and (19) and integrating $v_m = dx_m/dt$ over the time $t_m = fa/v_m$ that it takes the melt wave to travel the length a of the armature f times and rearranging, we get

$$V_c^2 = \frac{2\eta_r \rho Q w^2 L'}{\alpha\overline{\eta}_a \mu_0 M}\left(fa + \frac{2\alpha\mu_0 G}{\pi\eta_r} X_m\right) - 2\int_0^{t_m} V\mathcal{F}\, dt\,, \tag{20}$$

where X_m is the distance between the breech and the armature when the melt wave has destroyed the electrical contact. We identify V_c as the armature speed when transition occurs.

The thickness δ_m of the melted armature metal deposited in the rail, can be calculated as follows. On the assumption that the mass entrained on the rail equals the mass melted in the wave front, we obtain

$$\rho_s v_m \mathsf{h} = \rho_\ell (V + v_m)\delta_m \,,$$

where the subscripts s and ℓ denote the solid and liquid phases. Since $v_m \ll V$, this yields

$$\delta_m = \frac{v_m \rho_s}{V \rho_\ell}\,\mathsf{h}\,. \tag{21}$$

4. APPLICATION

Suppose that the armature metal is Aluminium and the rails are Copper then we need the following physical values, all expressed in SI units:

$\overline{\eta}_a = 7.2{\times}10^{-8}$, $\eta_r = 1.7{\times}10^{-8}$, $\rho_s = 2660$, $\rho_\ell = 2410$, $T_m - T_0 = 635$,
$Q = 9.67{\times}10^5$, $c_p(T_m - T_0)/Q = 0.589$, $\chi_a = 1.07{\times}10^{-4}$, $\chi_r = 1.16{\times}10^{-4}$.

With these values, equations (17) and (20) become

$$v_m = 1.19{\times}10^{-15}\frac{I^2 V}{w^2} - 6.68{\times}10^{-3}V\,, \qquad \mathsf{h} = \frac{1.85{\times}10^{-2}}{V}\,, \tag{22}$$

and

$$V_c^2 = 8.42{\times}10^{14}\frac{w^2 L'}{M}(fa + 6.67{\times}10^{-3}X_m)\,. \tag{23}$$

where we have omitted the drag term. The thickness of the deposited Aluminium follows from (21):

$$\delta_m = 1.1\frac{v_m}{V}\mathsf{h}. \tag{24}$$

To illustrate the theory, we shall apply it to a rail-gun experiment carried out in the Institute for Advanced Technology [6]. The armature's initial (free) width of 26 mm is compressed to 24.8 mm to fit between the rails. It follows that $f = 1.2{\times}10^{-3}/2\mathsf{h}$. Other typical values are: $w = 12.7\,\mathrm{mm}$, $a = 20.3\,\mathrm{mm}$, $I = 2.5{\times}10^5\,\mathrm{A}$, $V = 500\,\mathrm{m\,s^{-1}}$, and $L'/M = 2.2{\times}10^{-5}$. These yield:
$v_m = 0.45\,V = 225\,\mathrm{m\,s^{-1}}$, $\mathsf{h} = 37\,\mu\mathrm{m}$, $V_c = 1.00{\times}10^3\,\mathrm{m\,s^{-1}}$,
$\delta_m = 18\,\mu\mathrm{m}$, $t_m = 1.46\,\mathrm{ms}$, $X_m = 0.56\,\mathrm{m}$,
which values are in broad agreement with experiment.

Acknowledgement

Scientists at the IAT, University of Texas at Austin, especially Drs. Richard Marshall and Chadee Persad, have been most helpful with their extensive knowledge of rail-gun technology.

References

[1] J.P. Barber, A. Challita, B. Maas and L. Thurmond, "Contact Transition in Metal Armatures", *IEEE Trans. on Magnetics*, **27**. No. 1, pp. 228–232, 1991.

[2] J.P. Barber and A. Challita, "Velocity Effects on Metal Armature Contact Transition", *IEEE Trans. on Magnetics*, **29**, No. 1, 1993, 733–37, 1993.

[3] P.B. Parks, "Current Melt-Wave Model for Transitioning Solid Armatures", *J. Appl. Phys.*, **67**, No. 1, pp. 3511–16, 1990.

[4] T.E. James, "Current Wave and Magnetic Saw-Effect Phenomena in Solid Armatures", *7th EML Symposium*, San Diego, USA, April, 1994.

[5] L.C. Woods, *Kinetic Theory of Gases and Magnetoplasmas*, OUP, 1993, pp. 195–7.

[6] R.A. Marshall, C. Persad, K.A. Jamison, and M.J. Matyac, "Observations of Solid Armature Behaviour", *IEEE Trans. Magnetics*, **31**, No. 1, 214–18, 1995.

Progress Report on Research into Electromagnetic Launchers

An Armature / Rail Instability

February 1996

Professor L. C. Woods
University of Oxford
Mathematical Institute

An Armature / Rail Instability

Summary

It is known that the movement of a load along an beam, supported on an elastic foundation, will excite the beam into transverse vibrations that are particularly enhanced when the speed V of the load is close to the velocity of free waves in the beam. The lowest velocity at which a free wave can propagate defines the 'critical' velocity, which is given by

$$V_c = \left(\frac{4FEI}{\bar{\rho}^2}\right)^{\frac{1}{4}}, \tag{1}$$

where E is the modulus of elasticity of the beam, I is the beam's moment of inertia about its axis, F is the spring constant per unit length (restoring force due to the foundations) and $\bar{\rho}$ is the beam's mass per unit length. Unless there is damping present in the foundation, as $V \to V_c$, the amplitude of the forced disturbance increases without limit, i.e. we have an unstable resonance.

Experiments with rail guns, in which an Aluminium armature moves along copper rails at a speed exceeding a critical value V^*, have revealed a type of rail damage known as 'gouging'. Following the first gouge, there is a sequence of gouges on each rail that appear to be periodic, with a wave length that shortens with increasing distance along the rail. The magnetic force propelling the armature has components in the direction of the rails. Thus the armature is a load moving over two copper beams, each supported on a foundation material. This description raises the possibility of a connection between V_c for the rail/foundation system and the speed V^* at which gouging commences.

The amplitude of waves propagating along the rails at speeds of $V = \theta V_c$, depends on the physical parameters defined above and on the ratio θ. There are features of these waves in the neighbourhood of $\theta = 1$ that are particularly significant. We shall describe them for the case of an undamped system—the conclusions are unaltered for a small amount of damping. In a frame moving with the load, the waves appear as stationary standing waves, leading and trailing the position of the load. Let $x = 0$ define the position of the load, which is assumed to be moving in the positive direction along the OX-axis. The displacement y of the beam is reckoned to be positive if it is in the same direction as the load P acting on the beam. In the neighbourhood of $\theta = 1$, it has the values

$$\theta < 1: \quad y = \frac{Pk_c}{2\sqrt{2}\,F}\frac{\cos k_c x}{(1-\theta^2)^{\frac{1}{2}}}; \qquad \theta > 1: \quad y = -\frac{Pk_c}{2F}\frac{\sin k_c x}{(\theta^4-1)^{\frac{1}{2}}}, \tag{2}$$

where $k_c \equiv (F/EI)^{\frac{1}{4}}$.

In interpreting (2), we need to remember that there are two rails, i.e. two beams, and that the point loads correspond to the resultant forces acting on the surfaces of the armature in contact with the rail. For an Aluminium armature, we shall assume that the rails are displaced symmetrically about the centerline L

of the gun. In this case the armature moves steadily along L, without transverse oscillations. (The case of antisymmetrical displacements will be discussed at the end of this report.) For subcritical speeds, ($\theta < 1$), the first of (2) shows that the displacement is in the same direction as the load on each rail. Hence, with symmetrical displacements (see Fig. 2), the load tends to move the rails apart and allow freer passage for the armature along the gun. Provided this expansion is not so great that it interrupts the flow of current across the interface and causes transition, there will be no adverse consequences. In fact, as the rails separate, the load is reduced until a balance is attained between the force on the rails and the response of the elastic foundations, i.e. the rail/armature system is stable. However for speeds just supercritical, the second of (2) reveals that for $x > 0$, a position just in front of the resultant force, P, the rails are displaced *inwards*. Hence P is both increased and moved forwards. As the force increases, the inwards displacement becomes greater and P is increased further. Also, where the force between the rails and armature is greatest, will be the least resistance to the flow of the current across the interface. The copper will therefore be softened by the intense ohmic heating in this region. The hypothesis that this phenomenon *initiates* the periodic gouging of the rails, i.e. that $V_c = V^*$, appears to be plausible. The actual details of the gouging process remain to be elucidated; in this report we are considering only the trigger for the process.

At armature speeds greater than V_c, while the amplitude of the free waves is reduced, the gouging mechanism outlined above still applies. The length of the waves is reduced with increasing speed, so we would expect the gouge marks to appear closer and closer as the armature gathers speed. The reduction in wave amplitude *may* result in shallower gouge marks, but both the period and the depth of gouging require a more detailed mechanism for their explanation than we are presenting here.

One of the main difficulties in applying the theory lies in determining the response of the foundation, represented by F in (1). The usual approach is to treat the foundation as being a sequence of independent 'springs', but this is evidently a poor model of the actual physical process of the response of a continuous foundation material. The main original contribution in this report is a method of determining F. To do this we have had to find a local representation of a displacement that is distributed over the whole of the foundation material; approximations are unavoidable. For the IAT experiments in Austin, our method yields $V^* = 1380\,\mathrm{m/s}$, in good agreement with observations.

With Copper armatures, Dr. Richard Marshall has found a much lower value for V^*; under the same rail gun conditions, gouging begins at about 600 m/s. The Copper armature is 3.32 times heavier than an Aluminium armature of the same shape and this appears to be the only difference. In the theory outlined above, the mass of the armature has no role. However if *antisymmetric* displacements of the rail are induced by the greater mass, a much lower critical speed results. We shall discuss this in §5.

1. The Critical Armature Velocity

We base our account on the paper by J.T. Kenney [1], who cites several earlier works. A useful survey of the theory is presented by Graff [2]. There follows an outline of those parts of Kenney's paper, relevant to rail guns.

Let x denote the distance along the beam, y denote its transverse displacement and w be the load per unit length, as illustrated in Fig. 1. If M is the bending moment, then the classical relations

$$\frac{\partial^2}{\partial x^2}\left(EI\frac{\partial^2 y}{\partial x^2}\right) = -\frac{\partial^2 M}{\partial x^2} = w, \tag{3}$$

apply, provided the deflection y is relatively small. The several loads are given by

$$w = P(x,t) - \bar{\rho}\frac{\partial^2 y}{\partial t^2} - c\frac{\partial y}{\partial t} - Fy\,,$$

where $P(x,t)$ is the applied force and the other right hand terms are the inertia, damping and foundation loads. We have introduced $\bar{\rho}$, the mass per unit length, the damping coefficient c and the spring constant per unit length, F. The assumption here is that the response of the foundation can be represented *locally* by the force F. This is serious approximation, to which we shall return in §3. The differential equation for the beam is therefore

$$EI\frac{\partial^4 y}{\partial x^4} + \bar{\rho}\frac{\partial^2 y}{\partial t^2} + c\frac{\partial y}{\partial t} + Fy = P(x,t)\,. \tag{4}$$

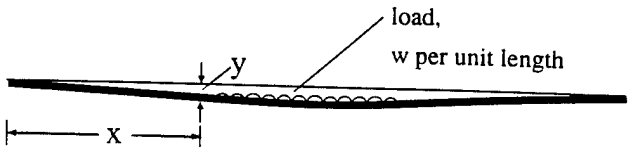

Figure 1: Deflection of beam by a load

We are interested in a possible resonance between an applied force moving along the beam with a velocity V, i.e. a force of the type $P(x,t) = P(x - Vt)$, and 'natural' waves that could exist in the beam in the absence of an applied force. Of course the force is required to excite these waves, but if in addition this force is resonant with natural frequencies, we can expect large amplitudes to result. To determine the natural waves, we seek wave-type solutions of the homogeneous, undamped form of (4), viz.

$$EI\frac{\partial^4 y}{\partial x^4} + \bar{\rho}\frac{\partial^2 y}{\partial t^2} + Fy = 0\,, \tag{5}$$

with $$y = Y\exp\{i(kx - \omega t)\} \qquad (Y = \text{const.}).$$

The dispersion relation is

$$EIk^4 - \bar{\rho}\omega^2 + F = 0\,. \tag{6}$$

Define $$\alpha \equiv (EI/F)k^4, \qquad \beta \equiv (\bar{\rho}^2/FEI)(\omega/k)^4\,, \tag{7}$$

then the wave length is $$\lambda = 2\pi/k = 2\pi(EI/F\alpha)^{\frac{1}{4}} \tag{8}$$

and (6) becomes $\alpha - (\alpha\beta)^{\frac{1}{2}} + 1 = 0\,,$

i.e. $$\beta = \alpha + 2 + \alpha^{-1}\,. \tag{9}$$

Since the phase velocity of the waves is $v_p = \omega/k$, we see that β determines v_p. To ensure propagating rather than evanescent waves, we require k to be real and therefore α to be positive. The lowest phase velocity occurs when the right-hand side of (9) is a minimum, which occurs at $\alpha = 1$, where $\beta = 4$. It follows that the lowest velocity at which a free wave can propagate is $v_p = V_c$, where

$$V_c = \left(\frac{4FEI}{\bar{\rho}^2}\right)^{\frac{1}{4}}\,. \tag{10}$$

Therefore resonance occurs when the load moves with this speed and from (7) and (8), the corresponding frequency and wave length are

$$\omega_c = (2F/\bar{\rho})^{\frac{1}{2}}, \qquad \lambda_c = 2\pi/k_c = 2\pi(EI/F)^{\frac{1}{4}}, \qquad k_c = (F/EI)^{\frac{1}{4}}\,. \tag{11}$$

2. Free standing waves

The next step in the analysis is to transform into a coordinate system moving with the load and then to investigate standing waves in this frame. This is effected by writing $x_1 = x - Vt$, $y_1 = y(x - Vt) = y_1(x_1)$ and then setting all partial derivatives with respect to time equal to zero. This simplifies equation (5) to

$$EIy^{iv} + \bar{\rho}V^2y'' + Fy = 0\,, \tag{12}$$

where the primes denote differentiation with respect to x_1. The load P does not appear on the right hand side, since it is now concentrated at the origin and enters the solution as a boundary condition, there being a discontinuity in shear across the origin of magnitude $-P/EI$. (Of course we could have included it in (12) as a delta function at the origin.) When damping is included, the general solution is complicated algebraically (see equation (14) of [1]), but for our present purposes it is sufficient to consider the undamped case.

We adopt the definitions

$$\theta \equiv V/V_c, \quad G^{\pm} \equiv \tfrac{1}{\sqrt{2}}\{(\theta^2+1)^{\frac{1}{2}} \pm (\theta^2-1)^{\frac{1}{2}}\}, \quad K \equiv \tfrac{1}{\sqrt{2}}(\theta^2+1)^{\frac{1}{2}}, \tag{13}$$

then the solution of (12) can be expressed (cf. equations (14a) and (14b) of [1])

$$\theta < 1: \quad y = \frac{Pk_c}{2\sqrt{2}F}\exp\{\pm k_s(1-\theta^2)^{\frac{1}{2}}\}\left\{\pm\frac{\sin Kk_cx}{\sqrt{2}K} + \frac{\cos Kk_cx}{(1-\theta^2)^{\frac{1}{2}}}\right\},$$

$$\theta > 1: \quad y = -\frac{Pk_c}{2F}\frac{\sin(k_cG^{\pm}x)}{(\theta^4-1)^{\frac{1}{2}}G^{\pm}} \qquad \begin{array}{ll} x < 0; & -\text{sign} \\ x > 0; & +\text{sign} \end{array}, \tag{14}$$

where the displacement y of the beam is positive if in the same direction as the force applied to the beam and we have introduced $k_s = k_c/\sqrt{2}$, the wave number for the static case, i.e. the wave number at $\theta = 0$.

Of course this solution is not valid *at* $\theta = 1$. Damping in the response of the foundation is required to suppress the infinity. Also observe that y and all its derivatives are continuous at the origin. In the neighbourhood of $\theta = 1$, we obtain the results given in (2).

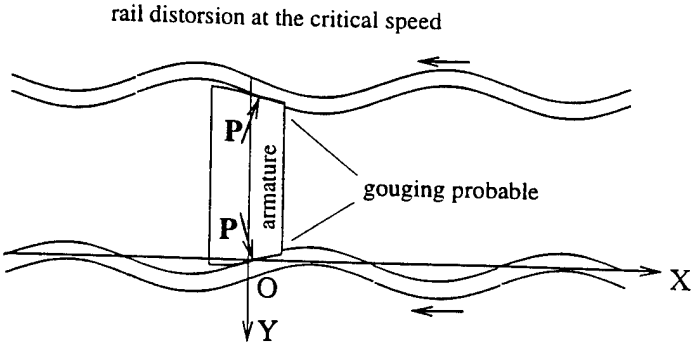

Figure 2: Armature gouging rails

The difference between the type of displacement for $\theta < 1$ and $\theta > 1$ is the key feature so far as gouging is concerned. For subcritical speeds, the displacement moves the rails apart until the load is sufficiently reduced for an equilibrium state to be achieved. The rail/armature system is stable. However for speeds just supercritical, for $x > 0$, the rails are displaced *inwards*. Hence the force is both increased and moved forwards. As the resultant force increases, the inwards displacement becomes greater and the force is further increased. The electrical contact between the rail and armature will have least resistance where the force is greatest, so we can expect ohmic heating to have softened the copper at this point. (At a temperature of 400° C, copper has only about a fifth of its room temperature tensile strength.)

Gouging may occur, as indicated in Fig. 2. Viewed in a frame with the armature stationary, the rail will 'snake' by, until the armature takes another

'bite' from the rail. In interpreting Fig. 2, it should be remembered that the waves shown are standing waves, stationary with respect to the armature. This process is repeated for the rest of the passage of the armature along the gun. What determines the gouging frequency is not yet explained, but as the armature continues to accelerate and θ increases, the wave length decreases, so we expect the gouging frequency to increase. Also the amplitude of the waves decreases, so—if the model is correct—we should see a reduction in the depth of the gouges along the rail.

3. Response of the foundation

The most difficult parameter to determine in the above theory is the amplitude of the spring constant F. In fact the foundation can only be roughly approximated by a series of independent, local springs. Our aim here is to find a good approximation to F.

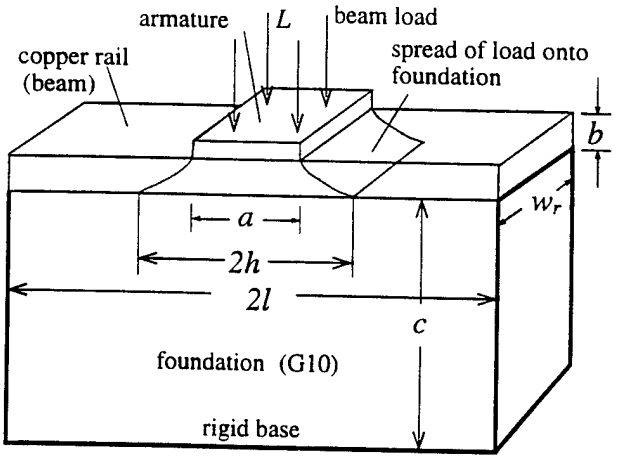

Figure 3: A rail gun beam and foundation

In Fig. 3 we give an overall picture of the load, beam and foundation, with the important dimensions identified. It is considerably out of scale. Figure 4 shows the compression of the foundation by a uniform load L applied to the beam over an infinite strip of width a. This load is transferred through the beam to the foundation. One problem that needs consideration is the distribution of pressure between the beam and the foundation. To avoid solving a complicated boundary value problem, at this stage we shall make a rough approximation by assuming that the load is equivalent in its effect to a uniform pressure p acting on the foundation over a range $2h$, where the relation between the length a of the armature and the distance h is to be determined.

For h we shall adopt the approximate relation

$$2h = a + b\,. \tag{15}$$

This means that the spread on each side of the load is equal to half of the thickness, b, of the copper beam. This empirical relation follows from Fig. 34 in the text by Timoshenko and Goodier [3], which figure is taken from a remarkable paper written in 1903 by Filon [4].[1]

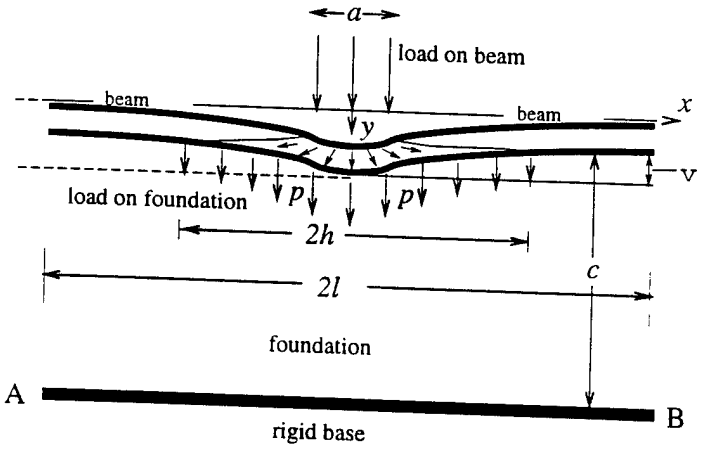

Figure 4: Strain of the foundation

As a first step to calculating F, we shall consider the problem shown in Fig. 5. There is a laminar of thickness c along OY and width $2l$ along OX. It has a rigid base on $y = 0$ and a uniform load on $y = c$, which exerts a pressure p on the beam, over a distance $2h$. The load is directed along the negative OY axis. We can replace the rigid boundary by mirroring the load in a similar laminar beneath the beam, for evidently the axis of such a system is straight, i.e. behaves as if it were rigid. We require the displacement v of the surface $y = c$. We shall deduce this by integrating the stress strain relation

$$\frac{\partial v}{\partial y} = \frac{1}{E_f}\{\sigma_y - \nu(\sigma_x + \sigma_z)\}\,, \tag{16}$$

in which ν is Poison's ratio and E_f is Young's modulus, for the foundation material. As the laminar extends infinity in the OZ direction, we can ignore the stress σ_z.

We introduce the dimensionless parameters

$$\alpha \equiv \frac{\pi c}{l}, \qquad \beta \equiv \frac{\pi h}{l}\,, \tag{17}$$

[1] Filon tackled the very difficult problem of determining the stress in a parallelopiped, subject to a distribution of forces on all sides. Some of the equations required more than one page for their presentation.

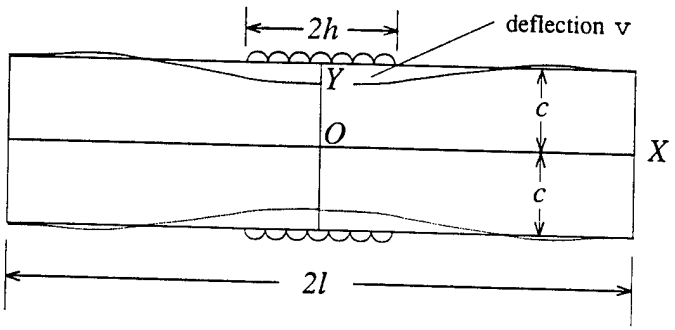

Figure 5: Laminar subject to symmetrical, concentrated loads

then find that the stresses are given by (cf. pp. 48–50 of [3])

$$\sigma_y = -\frac{ph}{l} - \frac{4p}{\pi}\sum_{m=1}^{\infty}\left\{\frac{m\alpha\cosh m\alpha + \sinh m\alpha}{\sinh 2m\alpha + 2m\alpha}\cosh(m\alpha y/c)\right.$$

$$\left. - \frac{(m\alpha y/c)\sinh(m\alpha y/c)\sinh m\alpha}{\sinh 2m\alpha + 2m\alpha}\right\}\cos(m\beta x/h)\,. \qquad (18)$$

To obtain σ_x is necessary only to change the signs of the indicated symbols. Integrating over $0 < y < c$, we find

$$v = -\frac{pc}{E}\frac{h}{l} - \frac{pc}{E}\Phi(x;\alpha,\beta)\,, \qquad (19)$$

where $$\Phi(x;\alpha,\beta) = \frac{8}{\pi}\sum_{m=1}^{\infty}\frac{1}{\alpha m^2}\left(\frac{\sinh^2\alpha m\sin\beta m}{\sinh 2m\alpha + 2m\alpha}\right)\cos(m\beta\frac{x}{h}).$$

We find from (19) that v changes sign, as indicated in Fig. 5, at $x = \pm kh$, where k is typically between 4 and 5. The average value of v, taken over its negative values is

$$|\overline{v}| = \frac{1}{2k}\int_{-k}^{k} v\, d(x/h)\,.$$

We shall therefore define F by

$$F|\overline{v}| = L/2h\,, \qquad L = 2hw_r p\,, \qquad (20)$$

where w_r is the width of the rail (see Fig. 3). Since we are ignoring stress in the OZ-direction, it does not matter whether the foundation is regarded as being a laminar, or an infinite collection of strips of width w_r, comprising the laminar. The quantity F is the restoring force acting on the beam due to a uniform displacement $\overline{v}$ of the foundation. This allows us to regard F as being a *local*, 'spring' force. It follows from (19) and (20) that

$$F = \frac{w_r E}{c\{(h/l) + \langle\Phi\rangle\}}\,, \qquad (21)$$

where $$\langle\Phi\rangle = \frac{1}{2k}\int_k^k \Phi(x/h;\alpha,\beta)\,d(x/h)\,.$$

There is one further approximation that should be mentioned. We have placed the load at the *center* of the beam to simplify the calculation; of course gouging will not necessarily occur at this position, but because h/l is typical very small, one expects that the resulting error will be negligible.

4. Application of the theory

The following values are taken from the rail-gun experiments at IAT, University of Texas at Austin. The dimensions shown in Fig. 3 are:

$a = 18.3\,\mathrm{mm},\ b = 6.35\,\mathrm{mm},\ c = 50.4\,\mathrm{mm},\ w_r = 31.75\,\mathrm{mm},\ l = 600\,\mathrm{mm}.$

For the physical properties we have: $E_f = 10^{10}\,\mathrm{Pa}$, $E_{cu} = 1.68{\times}10^{11}\,\mathrm{Pa}$, $\rho_f = 1900\,\mathrm{kg\,m^{-3}}$, $\rho_{cu} = 8960\,\mathrm{kg\,m^{-3}}$, $\rho_{al} = 2700\,\mathrm{kg\,m^{-3}}$, $\bar{\rho} = 1.81\,\mathrm{kg\,m^{-2}}$.

From these values and (15) and (17) we get $\alpha = 0.266$, $\beta = 0.0647$, $I = 6.77{\times}10^{-10}\,\mathrm{m^4}$, $EI = 114\,\mathrm{nt\,m^2}$. The following table sets out values of Φ as a function of x/h.

Table 1: The function $\Phi(x/h)$

x/h	0	0.2	0.4	0.6	0.8	1.0	1.2	1.4	1.6	1.8
$10^3\Phi$	621	615	597	565	513	416	316	257	212	176
x/h	2.0	2.2	2.4	2.6	2.8	3.0	3.5	4	4.5	5.0
$10^3\Phi$	146	121	99	81	65	51	24	5	-7	-16

We find $\Phi = 0$ at $x/h \approx 4.25$ and that its average over $(0, 4.25\,h)$ is 0.220. Thus from (21) we get $F = 2.61{\times}10^{10}$. Finally the critical speed follows from (1), viz.

$$V_c = \left(\frac{4FEI}{\bar{\rho}^2}\right)^{\frac{1}{4}}. \tag{22}$$

We find $V_c = V^* = 1,380\,\mathrm{m\,s^{-1}}$. In view of the approximations involved in determining the response of the foundation, this is closer to the experimental value of $\sim 1,400\,\mathrm{m\,s^{-1}}$ than we could expect; perhaps chance has played a role. Other consequences of the theory, such as the spacing of the gouge marks, their relationship on each rail (they should occur in a parallel formation), the dependence of V^* on the thickness b of the rails ($V^* \propto b^{\frac{3}{4}}$) and so on, should be tested against observation, before the theory can be adopted with confidence.

5. Copper armatures

The above theory appears to have some merit, since it offers an explanation of why gouging might occur and—for Aluminium armatures—arrives at a value of the critical speed in close agreement with observation. There remains one problem to consider. When the armature is made of Copper and all the other conditions remain the same, gouging sets in at speeds of only 600 m/s, well below the value obtained above. There are two possibilities: either the theory is wrong, or that Copper armatures behave differently, perhaps by exciting antisymmetrical displacements, as indicated in Fig. 6.

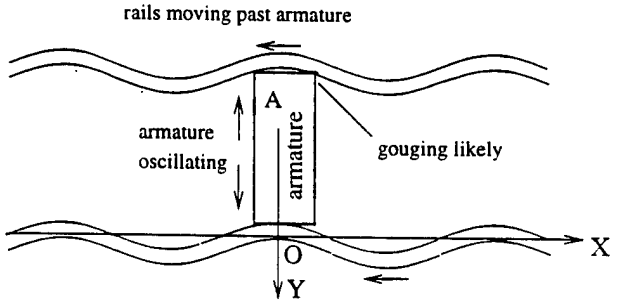

Figure 6: Antisymmetric displacements of the rails

Because its mass per unit length is greater than than of the rails supporting it, a Copper armature is vulnerable to small modulations in the straightness of the rails. It is therefore less likely to travel smoothly along the centerline of a rail gun than is a much lighter Aluminium armature. Transverse oscillations of the type indicated in Fig. 6 may be excited, and if the armature speed reaches a critical value, gouging becomes possible. We shall accept this description and determine a value for V_c, which we shall identify with V^*.

We now regard the armature, labelled A in Fig. 6, as being an additional concentrated mass M, on the beam and apply Newton's second law to it. As A moves between the rails, first one rail then the other provides the restoring force. There are two forces acting on A, namely the difference in shear across A in the rail that is decelerating the mass and the force due to the foundation behind that rail. The equation of motion for A is therefore

$$-EI\left[\frac{\partial^3 y}{\partial x^3}\right]_A - Fy = \hat{\rho} a \frac{\partial^2 y}{\partial t^2}\,, \tag{23}$$

where $[\cdots]_A$ denotes the jump in $\cdots$ and $\hat{\rho}$ is the mass of the armature plus rails per unit length. In order to obtain a rough estimate, we shall write

$$\frac{1}{a}\left[\frac{\partial^3 y}{\partial x^3}\right]_A \approx \left(\frac{\partial^4 y}{\partial x^4}\right)_A$$

which is exact in the limit as $a \to 0$. Now (23) assumes the form

$$EI\frac{\partial^4 y}{\partial x^4} + \hat{\rho}\frac{\partial^2 y}{\partial t^2} + Fy = 0\,, \tag{24}$$

which is identical with (5), with the modifications that $\hat{\rho}$ replaces $\bar{\rho}$ and that the equation applies to only to the armature and not to the whole rail-gun system. Despite this, it should give an estimate of the critical velocity for antisymmetrical displacements.

The theory is now the same as in §1, leading to equation (10):

$$V^* = \left(\frac{4FEI}{\hat{\rho}^2}\right)^{\frac{1}{4}}\,, \tag{25}$$

where

$$\hat{\rho} = 2\bar{\rho} + M/a\,.$$

The Aluminium armatures in the experiments cited in the previous section have a mass of 35.31 grm. A similar Copper armature would therefore have a mass of $M = 117\,\mathrm{grm}$. Hence, with the values qiven in §4, $\hat{\rho} = 2\bar{\rho} + M/a = 10.0\,\mathrm{kg\,m^{-2}}$. It follows from (25) that $V^* = 587\,\mathrm{m\,s^{-1}}$, in close agreement with Dr. Marshall's observations.

A simple test of this theory would be to load an Aluminium armature with heavy metal and see if this reproduces the value of V^* for a Copper armature. And other tests are suggested by the functional dependence exhibited in (22) and (25). If these tests confirm the theory, then the more difficult task of modeling the gouging process itself would the next step.

References

1. Kenney, J.T. (Jr.). 'Steady state vibrations of beam on elastic foundation for moving load.' *J. appl. Mech.* **21**, 1954, 359–64.
2. Graff, K.F. *Wave Motion in Elastic Solids*, Clarendon Press, Oxford, 1975, p. 175.
3. Timoshenko, S. and Goodier, J.N. *Theory of elasticity*, McGraw–Hill Book Co., 1951, pp. 46–50.
4. Filon, L.N.G. 'On an approximate solution for the beanding of a beam of rectangular cross-section, with special reference to points of concentrated or discontinuous loading'. *Trans. Roy. Soc. (London)*, Series A, **201**, 1903, 67–155.

Progress Report on Research into Electromagnetic Launchers

Three-Dimensional Effects on the Melt-Wave Model

May 1996

Professor L. C. Woods
University of Oxford
Mathematical Institute

Three-Dimensional Effects on the Melt-Wave Model

Summary

During my recent visit (26th April – 17th May, 1996) to IAT, I was shown a recovered armature, with a marked three-dimensional pattern of erosion, as indicated in Fig. 1 below – the contact surface of the armature was deeply wasted along its edges. To interpret this as due to a melt wave advancing from the rear of the armature would require a model in which the speed of the wave, v_m, was a function of the distance z, measured orthogonal to the direction of propagation.

The speed v_m is strongly dependent on the total current I flowing across the interface between the armature and the rail. In the two-dimensional model, this is treated as being independent of z. Let η_r be the rail resistivity, V the speed of the armature and μ_0 the permeability of free space, then $\delta_r = \eta_r/(\mu_0 V)$ is the very small diffusion length of the current measured in the direction of motion. If w denotes the depth of the surface of the armature in contact with a rail, the total current is $I = \delta_r w j_0$, where j_0 is the current density immediately in front of the melt-wave. The method adopted below to introduce three-dimensional effects into the melt-wave model, is to replace I by j_0 in the expression for v_m, and then to obtain an estimate of the distribution $j_0(z)$, using approximate diffusivity arguments. This approach allows most of the previous melt wave theory to be retained.

The report begins by describing a small numerical correction to the two-dimensional model presented in [1]. Then an expression for the minimum current required to initiate the melt wave and hence to provide the lubrication to allow the armature to move, is derived.

To improve on the diffusivity approach, it is necessary to undertake a *four-dimensional* (space and time) numerical calculation. A method of doing this, that does not involved more than three independent variables at each step, is described at the end of this report.

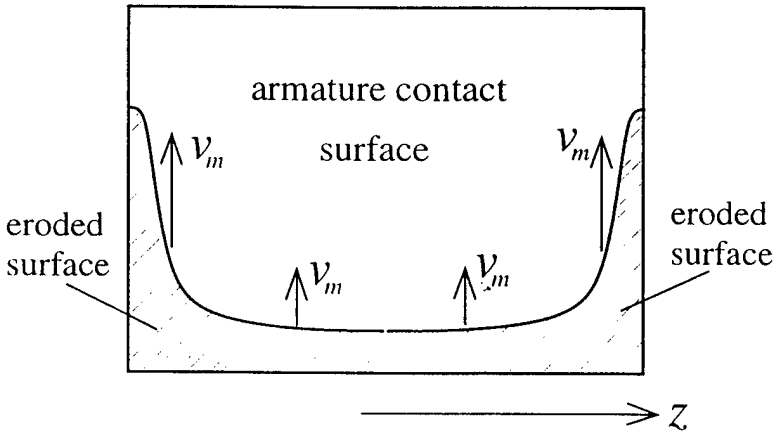

Figure 1: Erosion of armature due to three-dimensional currents

1. Some remarks about the two-dimensional model

In a correction made to the version of [1] presented at Baltimore, I have changed the value of the constant α appearing in the paper from an incorrect value of 1.148 to unity. The paragraph including equation (9) of that paper should now be replaced by:

> "....the sum over the separation parameter m of terms of the type
>
> $$j_y^r = A_m \cos(my/\delta_r)\, e^{\alpha x/\delta_r}\,, \tag{9}$$
>
> where $\alpha = \frac{1}{2}\{(1+4m^2)^{\frac{1}{2}}+1\}$ $(x<0,\ y<0)$.
>
> To determine m it is necessary to consider the diffusion of the electric current into the rail as viewed from the armature. In a time interval δt, a current element at $(x_0, 0)$ diffuses a distance $y = -(\xi_r \delta t)^{\frac{1}{2}}$ into the rail as it is convected a distance $x = V\delta t$ along OX. The element therefore moves along the parabola $y^2 = \delta_r(x - x_0)$. Thus, if $x_0 = -k^2 a$, $0 < k < 1$, is the distance between the melt wave and the front of the armature, $y = k(\delta_r a)^{\frac{1}{2}}$ is the value of y at which $j_y^r(0, y)$ is zero. Hence, by (9), the smallest value of m is $m_0 = \pi(\delta_r/a)/2k$. This corresponds to the smallest value of α, and hence, for a given (negative) value of x, it gives the dominant term in $j_y^r(x, 0)$. As δ_r/a is typically 10^{-3}, except for very small values of k, $m_0 \approx 0$ and $\alpha \approx 1$, which value we shall adopt."

With the modification just described, the velocity v_m of the melt wave and the depth h of the material melted (and hence presumably removed by adherence to the rail), is given by

$$v_m = \frac{\overline{\eta}_a \mu_0 I^2 V}{2\eta_r \rho Q w^2} - \frac{2\mu_0 G V}{\pi \eta_r}\,, \tag{2}$$

and

$$\mathsf{h} = \frac{\pi \eta_r}{2\mu_0 V}\,,$$

where

$$Q \equiv c_p(T_m - T_0) + L_m\,,\quad G \equiv \frac{c_p(T_m - T_0)}{Q}\chi_a\Big[1 + \Big(\frac{\chi_a}{\chi_r}\Big)^{\frac{1}{2}}\Big]\,. \tag{3}$$

In these expressions T_m is the melting temperature, T_0 is the laboratory temperature, $\overline{\eta}_a$ is resistivity in the solid armature, averaged over (T_m, T_0), η_r is the rail resistivity, I is the total current flowing through the armature, μ_0 is the permeability of free space, ρ is the armature density, w is the depth of the surface of the armature in contact with a rail, L_m is the enthalpy of fusion (latent heat),

c_p is the specific heat at constant pressure, χ_a, χ_r are the thermal diffusivities in the armature and rail, and V is the speed of the armature.

The total current I in (2) is related to the current density into the armature at the interface between the armature and rail, say j_0, by

$$I = w\delta_r j_0 \,. \tag{4}$$

Of the variables in (2), the only one that could depend strongly on z is the current density, j_0 implicit in I. It follows that, in order to model the erosion shown in Fig. 1, we must determine the z dependence of the current density across the interface.

Notice from (2) that the melt wave will not begin until a critical current given by

$$I^* = Kw \,, \tag{5}$$

where

$$K \equiv \left(\frac{4\rho Q G}{\pi \overline{\eta}_a}\right)^{\frac{1}{2}} ,$$

is attained. For copper rails and aluminium armatures, we find the values (in SI units): $G = 0.589$, $\overline{\eta}_a = 7.3{\times}10^{-8}$, $\chi_a = 1.07{\times}10^{-4}$, $\chi_r = 1.16{\times}10^{-4}$, $\rho = 2.66{\times}10^{3}$, $Q = 9.67{\times}10^{5}$. Substituting into (4), we get $K = 2.37{\times}10^{6}$. For example, with $w = 18.85{\times}10^{-3}$ m, the critical starting current is $I^* = 4.48{\times}10^{4}$ A. If it is necessary to lubricate the rails with liquid aluminium before it will move, then (5) gives the current necessary to start the armature in motion. It would of interest to use IAT experiments to check this speculation.

2. An semi-empirical treatment of the 3-D current

Figure 2 below shows a cross-section of a rail just behind an armature. The shaded area of this section indicates the region through which the current is flowing; the closer it is to the armature, the more this region will be distorted upwards. Our task is to obtain an estimate of the current distribution, $j_y(x, 0, z)$, through the interface on $y = 0$, between the rail and the armature. In the two-dimensional description of the melt wave given in [1], we had

$$j_y(x, 0) = j_0 e^{x/\delta_r} \qquad (x \text{ negative}) \,. \tag{6}$$

The only accurate method of determining a 3-D generalization of (6) is via a numerical solution, which requires time to be included as an independent variable. We shall outline a method of doing this in the following section. We should try to avoid this complication for each application, although some calculations will be necessary to support—or perhaps to eliminate—the empirical approach given here. The main difficulty in finding an analytical extension of (6) is that both *flow* and *diffusion* contribute to the three-dimensional effects.

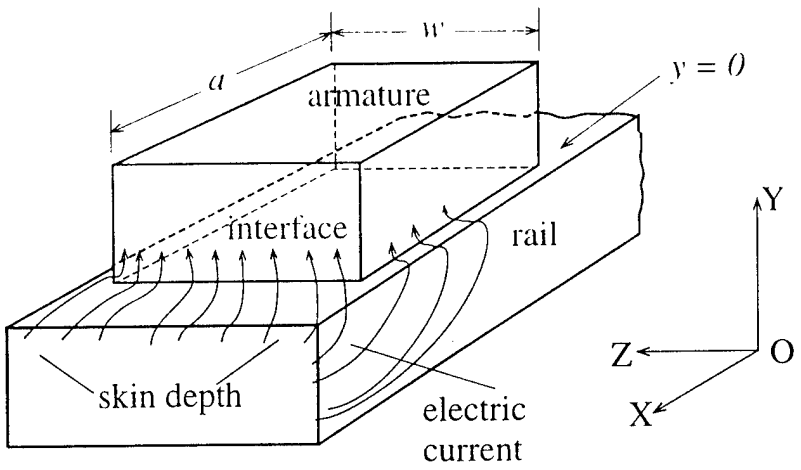

Figure 2: Three-dimensional currents across the rail/armature interface

Our method is to allow for diffusion by a factor $(1 + \beta \exp[|z|/\gamma])$, where the parameters β and γ are to be determined. Thus our hypothesis is that the normal current through the interface is given by an expression of the form

$$j_y(x, 0, z) = \alpha(1 + \beta e^{|z|/\gamma}) e^{x/\delta_r} . \tag{7}$$

The total current I passing through the armature is given by

$$I = 2 \int_0^{w/2} dz \int_{-\infty}^{0} j_y \, dx,$$

where w is the width of the armature (see Fig. 2). From (7)

$$I = \delta_r \alpha [w + 2\beta\gamma(e^{w/2\gamma} - 1)] . \tag{8}$$

In Fig. 3 we have sketched the current distribution at a fixed value of x. The 2-D distribution is flat, with the same area beneath it as the 3-D case. The skin depth in a section immediately below the armature, and at the position of the melt wave, is given by 2λ,[1] where

$$\lambda = (\xi_r t)^{\frac{1}{2}} = (\xi_r a/V)^{\frac{1}{2}} \qquad (\xi_r = \eta_r/\mu_0) , \tag{9}$$

in which ξ_r is the magnetic diffusivity in the rail and a is the length of the armature in contact with the rail. The time t is the armature transit time, since this is the time during whivh the rail is exposed to the current. The factor '2' takes care of the flow of the current layer from beneath the rail, as indicated in the figure.

[1] In copper, at room temperature, $\lambda \approx 0.116 t^{\frac{1}{2}}$, while at the melting temperature of aluminium, $\lambda \approx 0.219 t^{\frac{1}{2}}$.

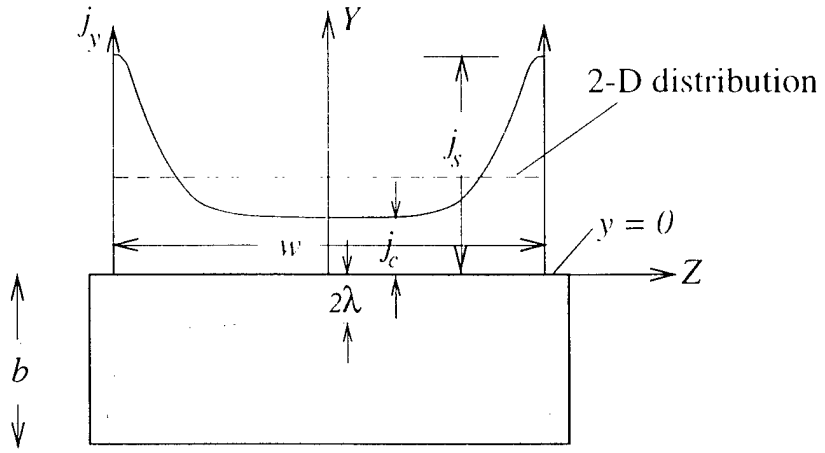

Figure 3: The current density distribution

We now assume that the current flowing up through the rail at a given point z is proportional to the depth of the rail carrying current, just before the flow turns "upwards" into the armature. Let j_s, j_c be the surface and central current densities, as shown in Fig. 3, then

$$\frac{j_s}{j_c} = f\frac{b}{2\lambda} = g\,, \quad \text{say}\,, \tag{10}$$

where b is the thickness of the rail and f is a form factor to allow for the distribution of the skin depth on the side of the rail. We expect this to be roughly triangular, with a thickness of λ at the top. This suggests a value $f = \frac{1}{2}$.

It follows from (7) and (10) that

$$\beta = \frac{g-1}{\exp(w/2\gamma) - g} \qquad (1 \le g \le e^{w/2\gamma}). \tag{11}$$

There remains the parameter γ. We shall assume that the edge current diffuses inwards and set γ equal to λ.

Summarizing, we now have

$$\left.\begin{aligned} j_y(x,0,z) \;&=\; \alpha(1+\beta e^{|z|/\lambda})\,e^{x/\delta_r} = j_0 e^{x/\delta_r}\,, \\ \text{where} \qquad \alpha \;&=\; \frac{I}{\delta_r\{w + 2\beta\lambda[\exp(w/2\lambda) - 1]\}}; \quad \beta = \frac{g-1}{\exp(w/2\lambda) - 1}\,. \end{aligned}\right\} \tag{12}$$

To apply the above theory to a railgun, we omit the second right-hand term in (2), since it is much smaller than the first. Then from (2), and (4) we get

$$p_m = \frac{\pi\overline{\eta}_a\delta_r^2}{4\rho Q\mathsf{h}}\,j_0^2\,,$$

which is independent of the width w of the armature. It is therefore an expression we can apply locally. It follows from (12) that

$$v_m = \frac{\pi \overline{\eta}_a \delta_r^2}{4\rho Q \mathsf{h}} \alpha^2 \left(1 + \beta e^{|z|/\lambda}\right)^2 . \tag{13}$$

The 2-D result is recovered at $\beta = 0$.

The dependence of v_m on z means that the melt-wave front will develop edge spurs, as shown in Fig. 1. The reason why we do not assume that the melt wave propagates *inward* from the spurs is that the length scales λ and δ_r appearing in (12) have very different magnitudes, which means that the current is concentrated at the smallest values of x, so the melt wave proceeds in the OX-direction rather than in the OZ-direction.

What is now required is a numerical evaluation of $j_y(x, 0, z)$ in typical conditions, in order to check the structure of the first equation in (12). In the following section, we shall outline a numerical method of doing this.

Illustration (using IAT values)

The temperature of the rail in the vicinity of the armature is required for an accurate determination of λ. We shall take the average of the values at room temperature and aluminium melting temperature, quoted in the footnote on page 5. At $a = 18.3\,\mathrm{mm}$, and $V = 500\,\mathrm{m\,s^{-1}}$, (9) gives $\lambda = 1\,\mathrm{mm}$. Take $f = \frac{1}{2}$ in (10). With $b = 6.35\,\mathrm{mm}$ ($\frac{1}{4}''$), we get $g = 1.59$, i.e. $j_s/j_c = 1.59$ (see Fig. 3). And with $w = 18.85\,\mathrm{mm}$, (12) gives $\beta = 0.59\exp(-w/2\lambda) = 4.71{\times}10^{-5}$. The current distribution is therefore

$$j_y(0, 0, z) = \alpha(1 + 0.59\exp\{(|z| - \tfrac{1}{2}w)\}) \qquad \text{(distances in mm)}.$$

The melt-wave velocity is

$$v_m \propto (1 + 0.59\exp\{(|z| - \tfrac{1}{2}w)\})^2 .$$

The speed on the edge of the armature is $1.59^2 = 2.53$ times faster than in the centre. Of course, these values are merely illustrative, since the factor f in (10) is really unknown and the ratio just calculated depends om f^2.

3. Numerical treatment of the 3-D current

In Fig. 4 we show a simple example of a railgun---one rail and half an armature, so that Σ is a surface of symmetry. The armature is at a distance $s = Vt$, where t is the elapsed time, more accurately,

$$s = \int_0^t V\,dt\,, \qquad ds = V\,dt\,. \tag{14}$$

It is convenient to use s in place of the time t.

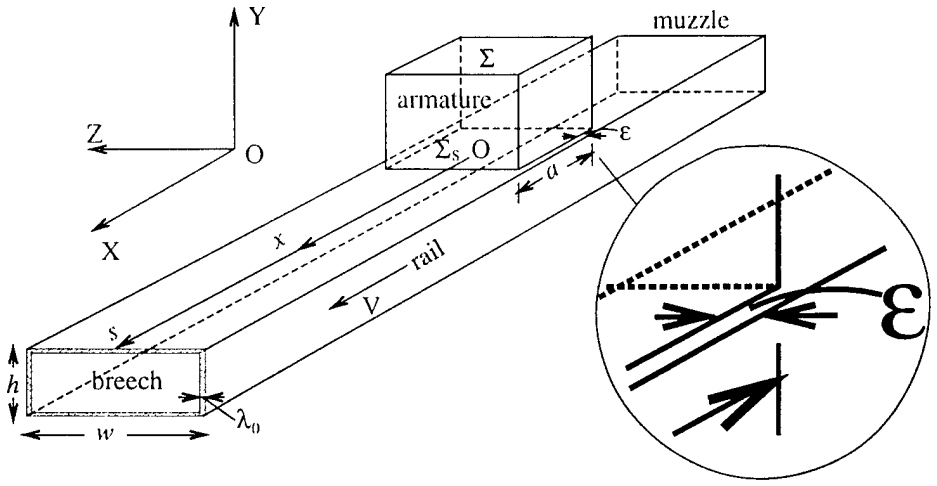

Figure 4: One rail and half the armature

The breech takes the initial current through a thin skin depth. For a small value of s, say s_0 corresponding to $t = t_0$, this is

$$\lambda_0 = (\xi_r t_0)^{\frac{1}{2}} . \tag{15}$$

At $t = 0$, the armature is stationary at the breech and the current density is momentarily infinite. It is therefore necessary to delay slightly before starting the calculation. At $t = t_0$, the cross-sectional area available to the current is (see Fig. 4) $2\lambda_s(w + h)$, so the initial current density has the components

$$j_x(t_0) = I(t_0)/\{2\lambda_0(w + h)\}, \quad j_y(t_0) = 0, \quad j_z(t_0) = 0 . \tag{16}$$

The boundary conditions for $\mathbf{j}$ are evident—no currents normal to the rail surface and symmetry across the surface Σ.

Relative to a frame fixed in the armature, the rail has a velocity along OX of V, for which case the curl of Ohm's law yields

$$\frac{\partial \mathbf{B}}{\partial t} + V\frac{\partial \mathbf{B}}{\partial x} = \xi \nabla^2 \mathbf{B} .$$

Since $\mu_0 \mathbf{j} = \boldsymbol{\nabla} \times \mathbf{B}$, the curl of this equation yields

$$\xi \nabla^2 \mathbf{j} = V\frac{\partial \mathbf{j}}{\partial x} + \frac{\partial \mathbf{j}}{\partial t} .$$

By (14) we have

$$\delta \nabla^2 \mathbf{j} = \frac{\partial \mathbf{j}}{\partial x} + \frac{\partial \mathbf{j}}{\partial s}, \qquad (\delta \equiv \xi_r / V = \delta(s)) . \tag{17}$$

Given $V(t)$, we find $s(t) = \int_0^t V(t)\, dt$, and invert this to get $t(s)$, then obtain $V(t(s))$. We must also ensure that

$$\boldsymbol{\nabla} \cdot \mathbf{j} = 0 . \tag{18}$$

The domain shown in Fig. 4 may be halved by using the symmetry about the OX-axis. Also it may be sufficiently accurate to terminate the domain about two armature lengths beyond the leading edge of the armature.

The armature/rail interface is the surface Σ_s, where (see figure), $\Sigma_s = (-a < x < 0,\ y = 0,\ -\frac{1}{2}w + e < z < \frac{1}{2}w - e)$. The task is to determine $\mathbf{j}(x, y, z, s)$, in particular to find $|j|$ on Σ_s. The boundary conditions should ensure that the total current entering the breech, also crosses Σ; this requirement will be a useful check on the calculations.

Four independent variables are one too many for practical calculation. The time variable s may be accommodated by the following iterative scheme. Start with the initial steady state,

$$\delta_0 \nabla^2 \mathbf{j}_0 = \frac{\partial \mathbf{j}_0}{\partial x}, \qquad s = s_0,\ V = V_0,\ \delta_0 = \xi_r / V_0\,,$$

then advance in small steps of s:

$$\begin{aligned} \delta_1 \nabla^2 \mathbf{j}_1 &= \frac{\partial \mathbf{j}_1}{\partial x} + \frac{\mathbf{j}_1 - \mathbf{j}_0}{\Delta s}, \qquad s = s_0 + \Delta s, \\ \ldots &= \ldots + \ldots\,, \\ \delta_n \nabla^2 \mathbf{j}_n &= \frac{\partial \mathbf{j}_n}{\partial x} + \frac{\mathbf{j}_n - \mathbf{j}_{n-1}}{\Delta s}, \qquad s = s_0 + n\Delta s\,, \end{aligned}$$

continuing until s equals the length of the rails. During each step, the condition

$$\frac{\partial j_{xn}}{\partial x} + \frac{\partial j_{yn}}{\partial y} + \frac{\partial j_{zn}}{\partial z} = 0\,,$$

must be satisfied.

Reference

1. Woods, L.C. "The current melt -wave model". *IEEE Trans. on Magnetics*, Vol 32, No. 1, ... 1997.

Progress Report on Research into Electromagnetic Launchers

Boundary Conditions Across a Rail / Armature Contact Surface

June 1996

Professor L. C. Woods
University of Oxford
Mathematical Institute

Boundary Conditions Across a Rail / Armature Contact Surface

Summary

In this report I shall give an account of the conclusions that I arrived at during my visit to IAT in May, concerning the averaged boundary conditions appropriate for a contact surface comprised of "a-spots". One aim was to obtain a macroscopic value for the resistivity, say η_{eff}, that could be used across the interface between the rail and armature in place of the "microscopic" details of the a-spots. This was followed by a calculation of the heat generated in the contact. The effect of relative motion between the rail and armature was then estimated and applied to the melt-wave model [1].

Since my visit, I have reconsidered the a-spot model and concluded that in the presence of a high speed of relative motion between the surfaces, it has little direct relevance to the *average* boundary conditions across the interface, except perhaps at the very beginning of the armature motion. I have therefore developed an 'asperity-plough' model, in which copper asperities plough through the armature material, smearing contact points that initially behave momentarily like a-spots, into narrow streaks, stretching from the site of the initial spot, backwards to the rear of the armature.

Provided the surfaces remain pressed together, the intense local heating at the asperities melts sufficient aluminium to allow the streaks to run together to form a continuous electrical contact between the rail and the armature. Thus we arrive at a model very similar to the melt-wave model, except that the ohmic heating is more intense due to the initial current concentration and the depth of material entrained on the rail depends on the size of the asperities, or equivalently, on the thickness of the contact layer and not on the skin depth of the electric current.

At the end of the report, we offer an explanation of the transverse striations visible on the entrained material, when both the rails and the armature are made of aluminium. It is very likely to be due to a shear-layer instability, such as that observed in the wing-tip streamers generated by high-flying aircraft in supercooled, atmospheric conditions.

1. The asperity-plough model

There are two distinct types of asperity—those consisting of copper intrusions into the aluminium armature (c-asperities) and the inverse type, i.e. those formed by aluminium intrusions into the copper rails (a-asperities). Figure 1 illustrates a c-asperity. We may suppose that initially, both types are equally numerous—of course this will depend on the smoothness to which the surfaces are finished. We would expect a-asperities to behave rather like a-spots; they move with the armature and are feed with current from the line of points immediately opposite on the rail. However, there are two reasons why the lifetime of a-asperities must be much shorter than that of c-asperities. First, at high temperatures, aluminium

has only a fraction of the shear strength of copper and secondly it melts at a much lower temperatures than copper. Thus, relative to c-asperities, a-asperities are sheared off quickly and even if they survive until melting, at this stage they immediately disappear by being entrained on the rail. This description implies that the current into the armature is largely transferred through c-asperities, or rather through the strips of molten aluminium generated by these asperities, as they plough through the armature during their transit towards its trailing edge. The distinction we are advancing between the two kinds of asperity receives some support by the observation that with aluminium armatures on aluminium rails, the appearance of the material entrained on the rails, with strong *transverse* striations, is very different from the standard copper rails (see §5 below).

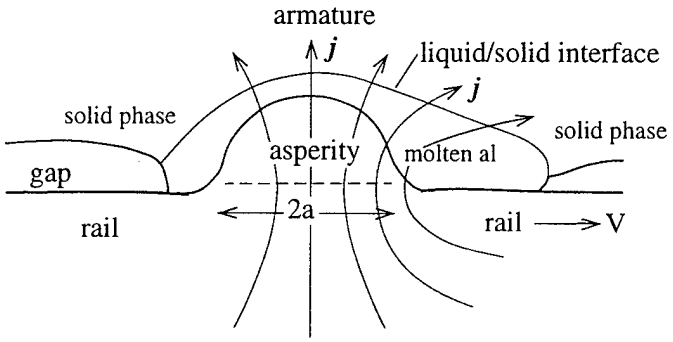

Figure 1: A copper asperity at an early stage

In Fig. 1 we show a copper asperity, C, at the stage when the current it carries has melted the surrounding aluminium. Because of the velocity skin effect, the dominant current-carrying asperities will begin their lives close to the trailing edge, TE, of the armature. Initially the current will be concentrated near the surface between C and TE, so there will be some melting in front of C. As C moves, it will leave behind it melted aluminium, but this will soon freeze on to the rail, leaving a high-resistance gap trailing it. Therefore, during the transit of C from its initial site to the trailing edge, there will be good electrical contact across a narrow strip extending, either from C's initial site to TE, or from a freeze-wave just behind C to TE. When C passes beyond TE, the strip will be entrained on the rail and carried away. This is illustrated in Fig. 2. However, it should be remarked that the figure is not even close to scale, since the spots are believed to be typically about 1/10 mm in diameter, with TE some two hundred times larger.

As the armature accelerates along the rails, more and more c-asperities are 'activated', until the strips they generate form a near-continuous region of good conductivity near the trailing edge of the armature. Provided the armature and rails continued to be pressed together, new, albeit shorter, asperities will be continue the process. But as the material near the rear of the armature is lost to the rails, the effective trailing edge will move forwards, in much the same way as the melt wave in the ideal contact model. On this model, we expect the

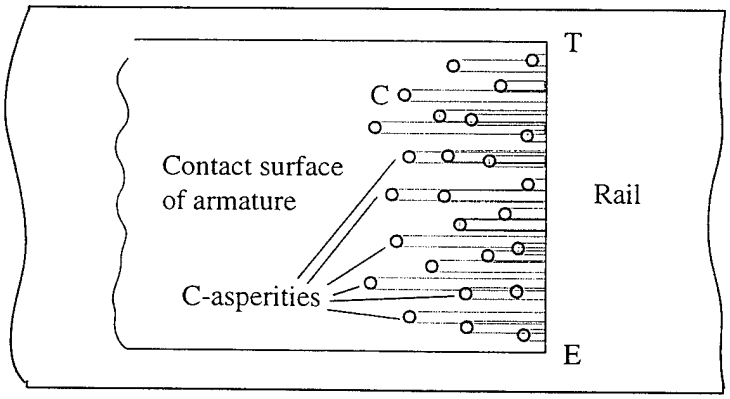

Figure 2: Conducting streaks generated by c-asperities

aluminium deposited on the rails to have a striated appearance; this can be seen in photographs of the rails [2] (also see Fig. 8).

2. Some results for the a-spot model

Since in the initial stages, the contact between the armature and rail will be through a-spots, we shall start by reviewing the theory of these spots. In the following, we shall adopt the subscript 's' to indicated values for a typical a-spot; quantities without a subscript will apply to the ideal (perfect contact) values.

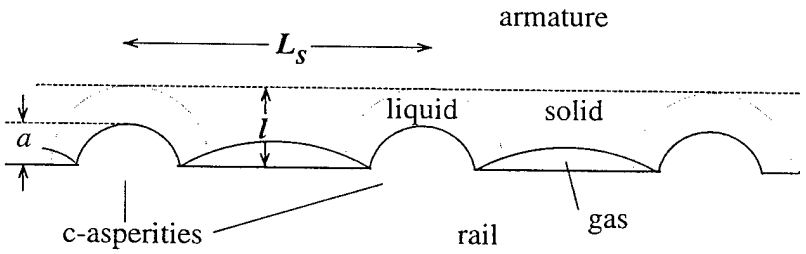

Figure 3: Idealized interface of c-asperities

Let A_s be the total area of solid or liquid contact between the armature and rail and A the actual or nominal area of the contact surface, then the ratio $\epsilon \equiv A_s/A$ will be much less than unity—values of 0.1 to 0.2 are suggested in the literature. Let F denote the normal pressure between the rail and armature, then the nominal pressure is $p = F/A$. For given metals, ϵ will depend on p and also on the surface temperature. Thus

$$\epsilon \equiv A_s/A, \qquad \epsilon = \epsilon(p, T)\,. \tag{1}$$

If I is the total current,

$$j_s = I/A_s, \quad j = I/A, \quad \text{so} \quad j_s = j/\epsilon\,. \tag{2}$$

Let η_s be the spot resistivity, then (see Fig. 3)

$$\eta_s = \frac{l-a}{l}\eta_a + \frac{a}{l}\eta_r\,, \tag{3}$$

where a is the average 'radius' of the asperities, l is the thickness of the interface layer, and η_a and η_r are the resistivities of the armature and rail. We shall assume that only the armature material is melted. At the melting temperature of aluminium (933 K), $\eta_a = 10.7{\times}10^{-8}\,\Omega\,\mathrm{m}$ and $\eta_r = 6.3{\times}10^{-8}\,\Omega\,\mathrm{m}$. The ratio a/l is not easy to estimate. Since η_s lies between η_r and η_a and these values are not wildly different, we shall be content to accept the average spot value, $\eta_s = 8.5{\times}10^{-8}\,\Omega\,\mathrm{m}$.

Let E denote the electric field across the layer, then

$$\eta_s j_s = E = \Delta V/l\,, \quad \Delta V = IR\,, \quad R = \eta_s l/A_s\,,$$

where R is both the layer resistance and the spot resistance. The effective resistivity for the layer therefore follows from

$$R = \frac{\eta_s l}{A_s} = \eta_{\text{eff}}\frac{l}{A}\,, \qquad \eta_{\text{eff}} = \eta_s/\epsilon\,. \tag{4}$$

Let N_s be the spot number density, then

$$N_s = \frac{A_s}{\pi a^2 A} = \frac{\epsilon}{\pi a^2}\,; \quad L_s = N_s^{-1/2}\,, \tag{5}$$

where a is the average spot radius and L_s is the spot spacing. Thus

$$\epsilon = \frac{\pi a^2}{L_s^2}\,. \tag{6}$$

To illustrate the theory, we shall adopt [3] $a = 0.5{\times}10^{-4}\,\mathrm{m}$ and $L_s = 2.3{\times}10^{-4}\,\mathrm{m}$, which gives $\epsilon \approx 0.15$ and $N_s \approx 2{\times}10^{7}\,\mathrm{m}^{-2}$. Hence from (4) and the estimate for η_s given above, $\eta_{\text{eff}} = 5.7{\times}10^{-7}\,\Omega\,\mathrm{m}$. The thickness of the transition layer is roughly $l \approx 2a \approx 100\,\mu\mathrm{m}$.

The spot magnetic diffusivity is $\xi_s = \eta_s/\mu_0 = 6.76{\times}10^{-2}$. For an individual spot, the diffusion time is

$$\tau_s = a^2/\xi = 0.25{\times}10^{-8}/6.76{\times}10^{-2} = 0.037\,\mu\mathrm{s}\,.$$

In a distance X there are $XN_s^{1/2}$ spots, but it is wrong to assume that the diffusion time for an armature of side X is simply the sum $XN_s^{1/2}\tau_s$, since after

each transition across a row of spots, a weaker field is presented to the next row. The correct diffusion time is

$$\tau_X = [2aXN_s^{1/2}]^2/\xi = \frac{4X^2}{\pi\xi}\epsilon\,. \tag{7}$$

For the perfect contact surface, $\tau_X = \tau_X^*$, say, has the value $\tau_X^* = X^2/\xi$. Omitting the factor $4/\pi$, we get $\tau_X \approx \epsilon\tau_X^*$, a physically obvious result.

3. Pinching and heating at the interface

It follows from the above, that to replace the a-spot model by a continuum representation, we need to introduce a thin interface layer, about 0.1 mm thick, in which the resistivity is about $1/\epsilon$ times the resistivity of molten aluminium. With $\epsilon = 0.15$, this amounts to a twenty-fold increase over the resistivity of the armature at room temperature. According to the melt-wave model, for an armature moving with a velocity V, the current density has the distribution $\mathrm{j} \propto \exp(x/\delta_r)$, where $\delta_r = \eta_r/(\mu_0 V)$ and x is negative, being the distance measured from the melt wave. In the layer just described, it would be necessary to replace δ_r by a number twenty times larger.

This raises the possibility that the magnetic field could diffuse rapidly between the armature and rail, allowing its pressure to completely break the electrical contact before the launch was completed. This would result in a pinched current, as illustrated in Fig. 4.

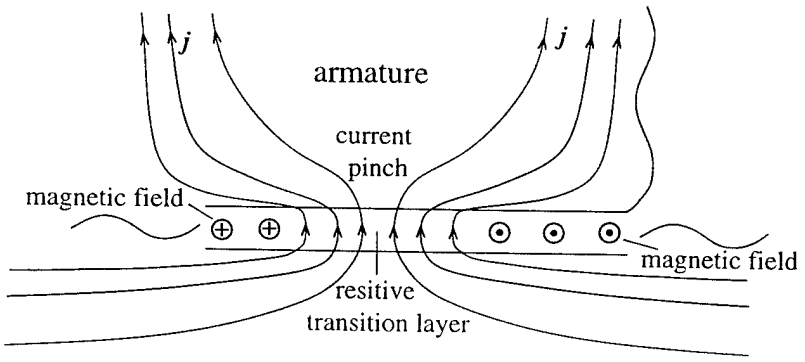

Figure 4: Current pinched by magnetic field

Consider the time required for the magnetic field to diffuse half way along an armature of length 18 mm. From (7)

$$\tau_X = \frac{4\times 18^2\times 10^{-6}}{\pi\times 6.76\times 10^{-2}}\times 0.15 = 910\,\mu\mathrm{s}\,.$$

But at a speed of, say, $V = 500\,\mathrm{m}s^{-1}$, the armature moves through 18 mm in $36\,\mu$s, i.e. the transition layer is renewed in this time. This means that there is insufficient time for the diffusion to take place. However, if $V \leq 20\,\mathrm{m}s^{-1}$, a pinch will develop.

The ohmic heating rate in a spot is $\eta_s j_s^2$ per unit volume. Hence for the whole surface, this rate is $\eta_s j_s^2 l A_s = \eta_s I^2 l / A_s$. Per unit volume of the corresponding continuum, this is

$$\frac{\eta_s I^2}{A_s A} = \frac{\eta_s I^2}{\epsilon A^2} = \frac{\eta_s}{\epsilon} j^2 = \eta_{\mathrm{eff}} j^2 .$$

In the example given above, this is twenty times greater than the rate in solid aluminium.

In the steady state—on the continuum description—the energy equation is

$$\nabla \cdot \mathbf{q} = \eta_{\mathrm{eff}} j^2 ,$$

where $\mathbf{q}$ is the heat flux vector. Integrating over a volume V, with an element $d\tau = l\, dS$, we get

$$\int_V \nabla \cdot \mathbf{q}\, d\tau = \int_{\partial V} \mathbf{n} \cdot \mathbf{q}\, dS = \eta_{\mathrm{eff}} j^2\, lA ,$$

where $\mathbf{n}$ is the outwards normal. Hence the jump in $\mathbf{q}$ across the surface is

$$\mathbf{n} \cdot [\mathbf{q}] = \eta_{\mathrm{eff}} j^2\, l ,$$

or

$$q_R - q_A = \eta_{\mathrm{eff}} j^2\, l . \tag{8}$$

4. Melt-wave interpretation of the asperity-plough model

As just described, the rate of melting in the neighbourhood of asperities is very much greater than in the ideal contact that formed the basis of the previous treatment of the melt wave model. By generating streaks of melted aluminium in the transition layer, close to the trailing edge of the armature, the c-asperities manage to cover a narrow region of the armature with a conducting fluid. The normal pressure between the rail and armature will help to spread this melt into a continuous layer. An irregular boundary will mark the leading edge of the collection of streaks, but shortly behind this, the streaks will run together, forming a continuous layer.

The average position of the boundary is a good approximation to a melt-wave front, the depth h of which is determined more by the thickness of the contact layer. than the penetration depth of the current distribution. Thus we arrive at a

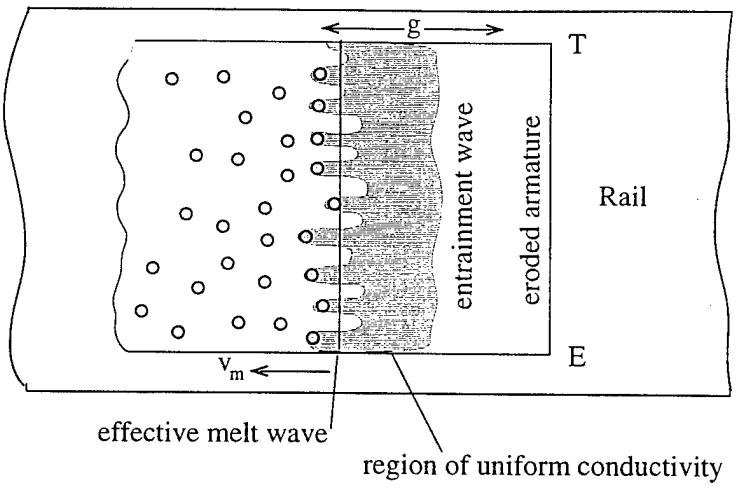

Figure 5: The asperity-plough model

model that is a mixture of a-spots and a continuum, as shown in Fig. 5. The rear of the narrow conduction strip is terminated by an air gap due to the entrainment of the melt on to the rail. Hence there will be an 'entrainment wave', advancing along the armature, close behind the effective melt wave.

We need an estimate for the width, g, of the region over which the aluminium remains liquid. In terms of the density density ρ, the specific heat c_p and the thermal conductivity κ, the thermal diffusivity is $\chi = \kappa/\rho c_p$. The initial width of the streaks of melted aluminium is $2a$ and the time for the heat to be (laterally) conducted through half this distance is $\tau_\kappa = a^2/\chi$. During this time the c-asperity will move through a distance

$$g = Va^2/\xi\,, \tag{9}$$

relative to the armature. For aluminium, $\chi = 1.07{\times}10^{-4}$, hence with $a = 0.5{\times}10^{-4}$, we get $g = 0.023V$ mm, i.e. at $V = 500\,\mathrm{m s^{-1}}$, $g \approx 12$ mm. This is much larger than the length scale for the electric current, which means that the aluminium strips will be a liquid long enough to merge into a continuous, conducting layer. However we do not expect the melted aluminium to fill the gap between the rail and armature surfaces over the whole width g. All that the model requires is a narrow region of uniform conductivity in which electrical contact is maintained.

Our model thus closely resembles an ideal melt wave. The fact that the melting initially occurs at *discrete* points on the armature, merely increases the heating rate. But we do require the force between the armature and rail to remain high enough for the melted aluminium to fill the gaps between the asperity streaks, as shown in Fig. 5.

The derivation of the melt velocity, v_m from the energy equation remains as given in [1], since the ragged leading edge has no effect on averages taken across the width of the armature. The only uncertainty is in the value to adopt for the

ohmic heating term. We shall replace the ideal average resistivity $\overline{\eta}_a$ appearing in the formula for v_m given in [1] by η^*. Thus

$$v_m = \frac{\pi\eta^* I^2}{2\rho Q w^2 \mathsf{h}} - \frac{G}{\mathsf{h}}\,, \tag{10}$$

where

$$Q \equiv c_p(T_m - T_0) + L_m\,, \qquad G \equiv \frac{c_p(T_m - T_0)}{Q}\chi_a\Big[1 + \Big(\frac{\chi_a}{\chi_r}\Big)^{\frac{1}{2}}\Big]\,. \tag{11}$$

An increase in the ohmic heating term is necessary, since the melting occurs largely at the c-asperities. With the ideal melt wave described in [1], we adopted $\eta^* = \overline{\eta}_a = 7.2{\times}10^{-8}$. The changes described in §2 imply that we should use the much larger value $\eta^* = \eta_{\text{eff}} = 8.5{\times}10^{-8}/\epsilon$. A difficulty arises with ϵ, which is largely unknown and varies across the region from a small value like 0.15 to unity. A simple average like $\epsilon \approx 0.5$ might be the best one can manage, short of a very detailed study.

Another uncertainty concerns the value to take for h. Above we suggested $\mathsf{h} = l$, where l is the thickness of the contact layer. In [1] we showed from mass conservation that the thickness of the entrained layer is given by $\delta_m = 1.1\mathsf{h}v_m/V$, which from (10) is fortunately independent of h. We may therefore use

$$\delta_m = 1.1\Big[\frac{\pi\eta^* I^2}{2\rho Q w^2 V} - \frac{G}{V}\Big]\,, \tag{12}$$

and measurements of δ_m, to determine η^*. This will provide a test of the theory.

5. Transverse striations observed on aluminium rails

In Fig. 6 we reproduce part of a photograph taken at IAT, University of Austin at Texas, showing the appearance of aluminium rails following the firing of an *aluminium* armature. The feature of interest here is the transverse gouges in the rail surface. From the figure we find that the wave length of the ridges is about 1mm. Apparently the melted aluminium at the contact surface has solidified into waves with their crests at right angles to the motion of the armature. It is a reasonable conjecture that these waves are generated by an instability in the sheared fluid layer separating the rail and armature. Vortex sheets are well-known to be unstable, a classic example being that observed in the wing-tip streamers generated by high-flying aircraft in supercooled, atmospheric conditions. Another is the generation of waves at the free surface of a liquid, over which a gas is flowing.

The subject has a long history, probably starting with Lord Rayleigh. For a recent treatment there is P.G. Saffman's monograph [4], from which the following results are taken.

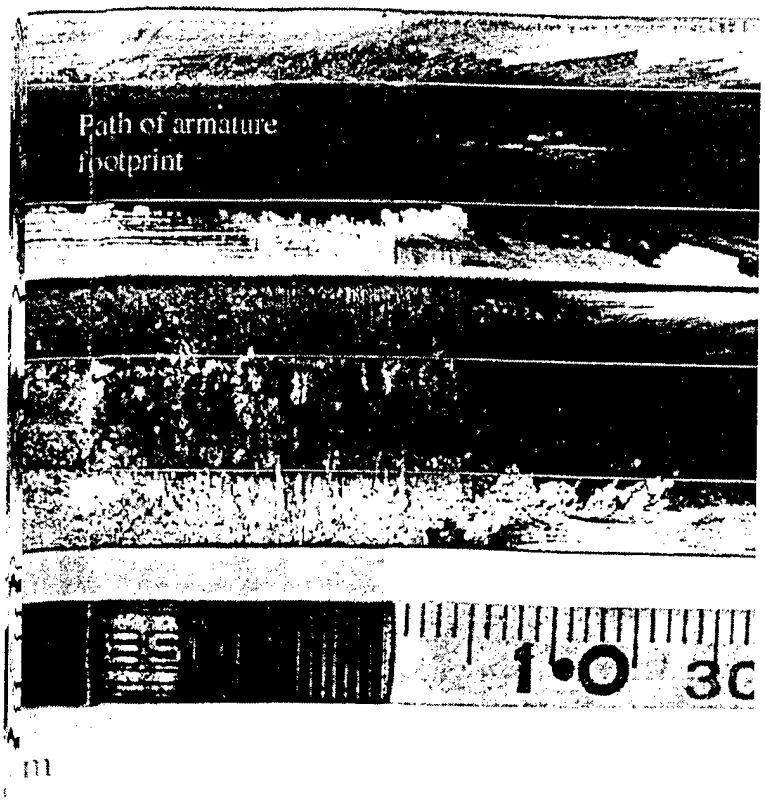

Figure 6: Transverse striations in aluminium rails

If the shear layer has a thickness h and a velocity jump of U (see Fig. 7), waves of length $\lambda = 2\pi/k$ have amplitudes proportional to $\exp(\sigma t)$, where the growth rate σ is given by

$$\sigma = \tfrac{1}{2}Uk\Big[(1 - \tfrac{1}{3}kh)(1 - kh)\Big]^{\frac{1}{2}}.$$

The validity of the theory requires that $h/\lambda \ll 1$, or $hk \ll 2\pi$.

Applying the theory to the sheared aluminium in the railgun, we identify h with h, the thickness of the contact layer and U with the velocity V of the armature. The waves most likely to appear are those given by the maximum growth rate, which occurs at $\mathsf{h}k \approx 0.634$ and has the value $\sigma \approx 0.170V/\mathsf{h}$. It follows from this that, after the passage of the armature, we should expect to see 'frozen' waves of wave length $\lambda = 2\pi\mathsf{h}/0.634 = 9.91\mathsf{h}$, provided the time scale $\tau_g = 5.88\mathsf{h}/V$ for their growth is comparable with the time it takes for the armature to be displaced through half a wave length, viz. $\tau_\lambda = 4.96\mathsf{h}/V$. This resonance condition is evidently met.

If we accept the estimate mentioned in §2, namely $l = 0.1$mm and set h equal to l, we arrive at $\lambda \approx 1$mm, which appears to be supported by Fig. 6.

Incidently, the same experiment at a later time, shows clear examples of the

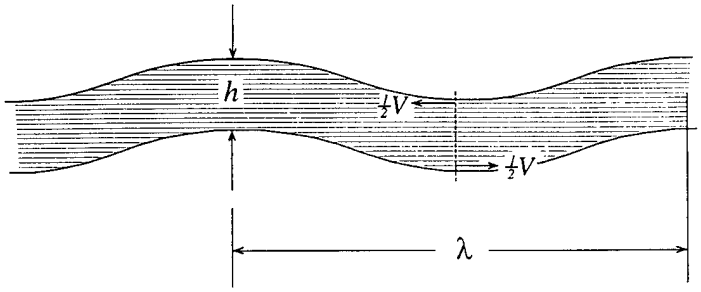

Figure 7: Vortex sheet instability

parallel striations caused by aluminium asperities. These are shown in Fig. 8, p. 12. The striations are about 0.5mm apart and their width is perhaps a half of this distance, values that correspond to $a = 1.25\times10^{-4}$ m and $L_s = 5\times10^{-4}$ m, which is about twice the estimates given in §2 (following equation (6)).

References

1. Woods, L.C. "The current melt -wave model". *IEEE Trans. on Magnetics*, Vol 32, No. 1, Jan. 1997.
2. IAT experiment; results supplied by Dr. Chadee Persad.
3. Kim, Y.M., Bourell, D.L. and Persad, C. "Consolidation of metallic glass ribbons using electrical discharge welding". *Metallurgical Trans. A*, Vol 19A, June 1988.
4. Saffman, P.G. *Vortex Dynamics*. Cambridge Monographs on Mechanics and Applied Mathematics, 1992, p. 163.

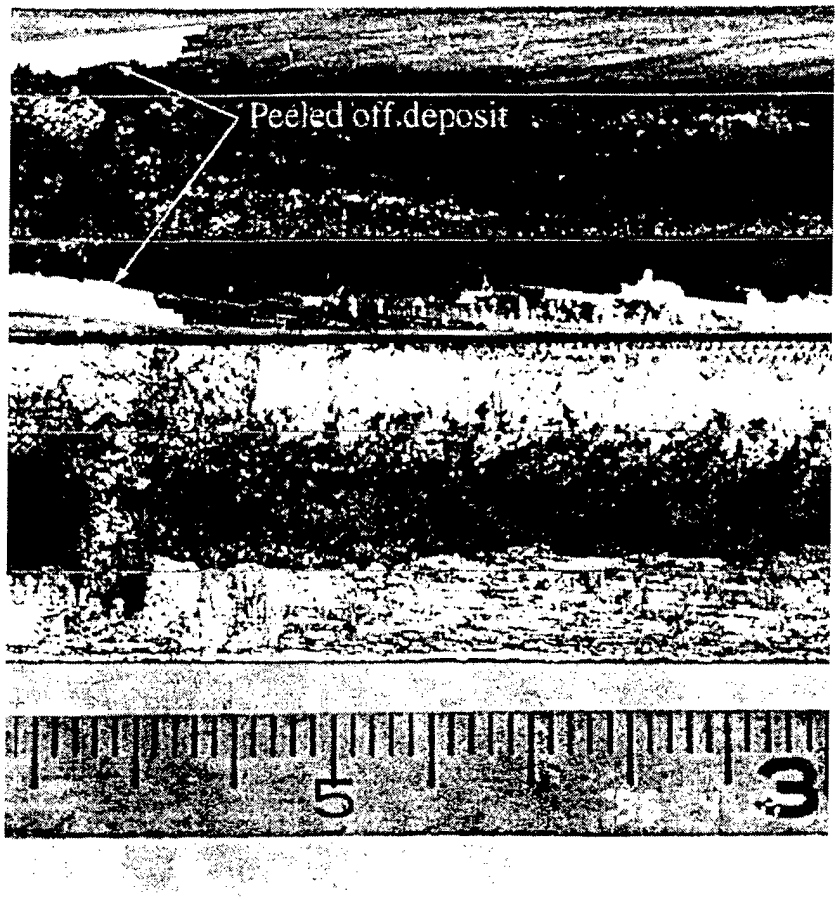

Figure 8: Some evidence of streaks generated by a-asperities

Distribution List

Administrator
Defense Technical Information Center
Attn: DTIC-DDA
8725 John J. Kingman Road, Ste 0944
Ft. Belvoir, VA 22060-6218

Director
U.S. Army Research Laboratory
Attn: AMSRL-WT-PB (Edward Schmidt)
APG, MD 21005-5066

Dr. John P. Barber
IAP Research, Incorporated
2763 Culver Avenue
Dayton, OH 45429-3723

Office of the Assistant Secretary
of the Army (RDA)
Attn: Dr. Richard Chait
Deputy Asst. Secretary of the
Army for Research & Technology
The Pentagon, Room 3E374
Washington, DC 20310-0103

Robert J. Taylor
Lockheed Martin Vought Systems
M/S: WT-21
P.O. Box 650003
Dallas, TX 75265-0003

Dr. Keith A. Jamison
Science Applications International Corp.
1247-B N. Eglin Parkway
P. O. Box 126
Shalimar, FL 32579

Director
Army Research Office
Attn: Gerald J. Iafrate
P.O. Box 12211
Research Triangle Park, NC 27709-2211

Commander
U.S. Army Armament Research,
Development and Engineering Center
Attn: AMSTA-AR-CCL (Bob Schlenner)
Bldg. 65N
Picatinny Arsenal, NJ 07806-5000

Russ Klug
Wright Laboratories
WL/ MNMW
Eglin AFB, FL 32542

Commander
U.S. Army Armament Research,
Development and Engineering Center
Attn: AMSTA-AR-FS (Ted Gora) Bldg. 94
Picatinny Arsenal, NJ 07806-5000

Dr. Ingo W. May
Office of the Director
Army Research Laboratory
ATTN: AMSRL -WT
Army Research Laboratory
APG, MD 20115-5066

Mr. Dennis Hildenbrand
PKD New Jersey
520 Speedwell Ave., Suite 108
Morris Plains, NJ 07950

George Chryssomalis
SAIC
3800 W. 80th St., Suite 1090
Bloomington, MN 55431

Dr. Robert Guenther
Army Research Office
P.O. Box 12211
Research Triangle Park, NC 27709-2211

Alex Zielinski
U.S. Army Research Laboratory
AMSRL-WT-PB, B390, RM 212
APG, MD 21005-5066

Dan Dakin
Science Applications International Corp.
2200 Powell St., Suite 1090
Emeryville, CA 94608

Mr. Albert Horst
Chief, Propulsion and Flight Division
Army Research Laboratory
ATTN: AMSRL -WT-P
Army Research Laboratory
APG, MD 20115-5066

Director
US Army Research Lab
ATTN: AMSRL OP SD TA
2800 Powder Mill Road
Adelphi, MD 20783-1145

Commander
U.S. Army Armament Research,
Development and Engineering Center
Attn: SMCAR-FSE (Dennis Ladd) Bldg. 382
Picatinny Arsenal, NJ 07806-5000

Raymond C. Zowarka
Center for Electromechanics
The University of Texas at Austin
Pickle Research Campus
EME 13, C R 7000
Austin, TX 78712

Director
US Army Research Lab
ATTN: AMSRL OP SD TL
2800 Powder Mill Road
Adelphi, MD 20783-1145

Distribution List

Director
US Army Research Lab
ATTN: AMSRL OP SD TP
2800 Powder Mill Road
Adelphi, MD 20783-1145

Director
U.S Army Research Laboratory
Attn: AMSRL-WT-PD (Dr. Bruce Burns)
Bldg. 390
APG, MD 21005-5066

Director
U.S Army Research Laboratory
Attn: AMSRL-WT-WD (Dr. John Powell)
Bldg. 120
APG, MD 21005-5066

Director
Army Research Laboratory
AMSRL-CI-LP
Technical Library 305
APG, MD 21005-5066